NUMERICAL METHODS FOR THE CALCULATION OF THREE-DIMENSIONAL NOZZLE EXHAUST FLOW FIELDS*

By Sanford M. Dash and Paul D. Del Guidice
Advanced Technology Laboratories, Inc.

SUMMARY

Two numerical codes have been developed for the calculation of three-dimensional nozzle exhaust flow fields associated with hypersonic airbreathing aircraft. Both codes employ reference plane grid networks with respect to three coordinate systems. Program CHAR3D is a characteristic code utilizing a new wave preserving network within the reference planes, while program BIGMAC is a finite difference code utilizing conservation variables and a one-sided difference algorithm. Secondary waves are numerically captured by both codes, while the underexpansion shock and plume boundary are treated discretely. The exhaust gas properties consist of hydrogen-air combustion product mixtures in local chemical equilibrium. Nozzle contours are treated by a newly developed geometry package based on dual cubic splines. Results are presented for simple configurations demonstrating two- and three-dimensional multiple wave interactions.

INTRODUCTION

Hypersonic aircraft with airbreathing propulsion will require a high degree of engine/airframe integration in order to achieve optimized performance. The engine exhaust flow, because of physical area limitations, will generally be underexpanded at the nozzle exit, and in order to obtain maximum propulsive efficiency, the vehicle afterbody undersurface is used to provide additional expansion. This results in a three-dimensional nozzle flow whose boundaries are defined both by the solid boundary of the nozzle wall and by the boundary separating the nozzle flow from the vehicle external flow. A typical exhaust nozzle (fig. 1) may be characterized as having nozzle modules with cross sections which are rectangular in shape. These nozzles may be arranged in multiples and discharge into a common nozzle. The flow fields to be analyzed start at the combustor exit and each module may be analyzed individually until its merger with adjacent modules and the external flow field.

*This research was performed under Contract No. NAS 1-12726.

In developing a numerical model for this flow field, the following dominant features must be accounted for:

(1) The flow properties at the combustor exit are highly nonuniform. Burning and mixing in the combustor yield regions of highly varying composition, temperature, and stagnation properties. In addition, shock waves are produced in the vicinity of the injectors. Although the strength of these waves decays rapidly as they propagate through the burner, they are generally present at the burner exit and must be accounted for.

(2) The exhaust gas mixture consists of hydrogen-air combustion products and significant burning may still occur in the initial regions of nozzle expansion.

(3) The flow field geometry is quite complex. The engine modules consist of multiple surfaces with sharp interior corners, and flow fences to contain the external exhaust flow may be present.

(4) The interior nozzle flow field is dominated by complex wave interactions with waves generated and reflected off multiple surfaces. In addition, sharp interior corner regions must be accounted for.

(5) The nozzle exhaust flow interacts with the nonuniform vehicle external flow field. This complex interaction for underexpanded exhaust flows results in an expansion system propagating toward the vehicle undersurface from the cowl trailing edge and a spanwise expansion generated by the sidewall interaction. An underexpansion shock propagates outward into the nonuniform vehicle external flow, and the exhaust and external flow are separated by a plume boundary. In addition, pressure and flow deflection mismatch between adjacent modules may occur, resulting in a spanwise multiple shock system.

To best accommodate highly rotational variable composition flow fields, a grid network which follows streamlines is preferred. For nonstreamline networks, large errors may be associated with streamline interpolation procedures for nonequilibrium flow calculations, as discussed by Sedney (ref. 1). For two-dimensional flow fields, a grid network following the flow streamlines is readily obtained. Such a system is employed in references 2 and 3 for the calculation of chemical reacting nozzle flow fields and supersonic combustor flow fields, employing a "viscous" characteristics technique. In this approach, a uniform marching step Δx is taken, new streamline grid points are obtained, and characteristic data are obtained by interpolation on the initial data line. Such a scheme can readily be extended to three dimensions via the reference plane approach. This approach involves the definition of a reference plane system in which the three-dimensional volume under consideration is spanned by an appropriately selected series of planes which intersect the boundaries of the considered volume. The equations of motion within the reference planes are expressed in a quasi-streamline coordinate system,

where quasi-streamlines are the projections of the actual stream surfaces onto these reference planes. Then, although the actual streamlines are not traced, streamline interpolation procedures are minimized.

In addition to minimizing streamline interpolation procedures, use of the reference plane approach has other distinct advantages. By developing the equations of motion with respect to different reference plane systems (Cartesian, cylindrical, and line source), complex geometric configurations may be analyzed. In figure 2(a), a reference plane network is depicted for a typical nozzle module, wherein the line source system shown alleviates the need for adding reference planes as the sidewall opens. The addition or deletion of reference planes is provided for automatically, based on their proximity to walls. A more complex situation is depicted in figure 2(b) for the flow field downstream of the modules. For this calculation, a combination of several systems is employed and provisions are included for automatic switching from one system to another as the character of the boundary surfaces changes. The reference plane system also caters to the usage of reference plane characteristics at all boundary points. This approach is generally recognized as the most accurate boundary calculational procedure (ref. 4). However, it proves cumbersome when employed in conjunction with nonreference plane networks due to the complex interpolation procedures then required.

The reference plane characteristic technique has been widely used for the calculation of three-dimensional supersonic flow fields, and the authors had previously developed a program employing this technique for the calculation of nozzle exhaust flow fields (refs. 5 and 6), which is in current usage at NASA Langley Research Center (refs. 7 and 8). That program, as well as most reference plane characteristic (refchar) codes in common usage (refs. 9 and 10), employs an inverse scheme wherein interpolations are performed to obtain data at the intersection of the quasi-characteristics with the initial data surface. Comparisons of such refchar codes with shock capturing finite difference codes (ref. 11) have led to the general conclusion that such difference codes are better able to analyze complex flow fields with multiple secondary shocks. From experience gained with the authors' original refchar code, it was felt that the inability to successfully analyze such flow fields was primarily due to the inverse interpolation procedures employed. Such procedures tend to ignore the presence of weak waves by allowing the quasi-characteristic lines to arbitrarily cross each other. The numerical diffusion associated with these interpolations can become significant, particularly when the local Courant number (ratio of overall marching step to local maximum allowable marching step) is much less than one. The smearing of these weak waves is enhanced by resorting to higher order interpolations on the initial data line.

To treat complex multiwave flow fields and still retain the advantages that reference plane methods afford, two new numerical codes have been developed. Program CHAR3D

is a refchar code which employs the wave preserving network depicted in figure 3(a) as compared to the standard inverse network of figure 3(b). This new network tends to preserve wave systems and secondary shock waves have been successfully captured with it with a minimum of smearing. In addition, CHAR3D employs a nonisentropic pressure-density relation along streamlines to calculate shock entropy losses and utilizes conservation variables in constructing derivatives normal to the reference plane. Program BIGMAC is a reference plane finite difference code utilizing a quasi-streamline grid in the reference planes as depicted in figure 3(c). BIGMAC captures shock waves via the use of conservation variables in conjunction with a one-sided difference algorithm.

SYMBOLS

a_e	equilibrium sound speed, ft/sec (m/sec)
C_v	specific heat at constant volume
E(k)	conservation variables (k = 1 to 6) defined in text (see eq. (1))
F(k)	conservation variables (k = 1 to 6) defined in text (see eq. (1))
G(k)	conservation variables (k = 1 to 6) defined in text (see eq. (1))
H(k)	conservation variables (k = 1 to 6) defined in text (see eq. (1))
H	stagnation enthalpy, ft^2/sec^2 (m^2/sec^2)
h	static enthalpy, ft^2/sec^2 (m^2/sec^2)
h_1, h_2, h_3	defined in text (see eq. (1))
I	index of data point in reference plane
J	index of reference plane
J_1, J_2	defined in text (see eq. (1))
K	index of marching step
M	Mach number in reference plane, q/a_e

$\hat{n}$	unit normal to surface
P	pressure, lb/ft^2 (N/m^2)
q	magnitude of velocity in reference plane, ft/sec (m/sec)
S	entropy, $ft^2/sec^2\text{-}^oR$ $(m^2/sec^2\text{-}K)$
T	temperature, ^oR (K)
$\vec{V}$	flow velocity vector
u	velocity component in marching direction in reference plane, ft/sec (m/sec)
v	velocity component normal to reference plane, ft/sec (m/sec)
w	velocity component in reference plane normal to marching direction, ft/sec (m/sec)
x,y,z	Cartesian coordinates
r,θ,z	line source coordinates
x,θ,r	cylindrical coordinates
Γ	equilibrium isentropic exponent
ρ	density, $slugs/ft^3$ (kg/m^3)
Φ	fuel-air equivalence ratio
ϕ	velocity direction in reference plane, rad
ψ	velocity direction with respect to reference planes, rad

Arrows over symbols denote vector quantities. Coordinate subscripts denote differentiation with respect to the coordinate.

GOVERNING EQUATIONS

Program BIGMAC

The equations of motion for the steady inviscid flow of a gas mixture in chemical equilibrium, written in conservation form with respect to the streamline reference plane system described, are:

$$\vec{E}_x + \vec{F}_y + \vec{G}_z + \vec{H} - \frac{h_1}{h_3}\frac{w}{u}\vec{E}_z - \frac{h_2}{h_3}\vec{F}_z \tan\alpha = 0 \tag{1}$$

where $\tan\alpha$ is $\partial z/\partial y$ at constant x and for $k = 1$ to 6

$$\vec{E}(k) = h_2h_3\begin{vmatrix} \rho u \\ P + \rho u^2 \\ \rho uv \\ \rho uw \\ \rho uH \\ \rho u\Phi \end{vmatrix} \qquad \vec{F}(k) = h_1h_3\begin{vmatrix} \rho v \\ \rho uv \\ P + \rho v^2 \\ \rho vw \\ \rho vH \\ \rho v\Phi \end{vmatrix}$$

$$\vec{G}(k) = h_1h_2\begin{vmatrix} \rho w \\ \rho uw \\ \rho vw \\ P + \rho w^2 \\ \rho wH \\ \rho w\Phi \end{vmatrix} \qquad \vec{H}(k) = \begin{vmatrix} 0 \\ -J_1h_3(P + \rho v^2) \\ (J_1h_3u + J_2h_1w)\rho v \\ -J_2h_1(P + \rho v^2) \\ 0 \\ 0 \end{vmatrix}$$

System	J_1	J_2	h_1	h_2	h_3
Cartesian	0	0	1	1	1
Line source	1	0	1	x	1
Cylindrical	0	1	1	z	1

Program CHAR3D

In nonconservation form, these equations (in continuous regions of the flow field) may be written

$$\left.\begin{aligned} &\nabla \cdot (\rho \vec{V}) = 0 \\ &\rho(\vec{V} \cdot \nabla)\vec{V} + \nabla P = 0 \\ &\vec{V} \cdot \nabla H = 0 \\ &\vec{V} \cdot \nabla \Phi = 0 \end{aligned}\right\} \tag{2}$$

The equations may be cast in characteristic form with respect to the reference plane systems described by writing the above equations in scalar form and transposing those terms not involving variations in the x- or z-direction onto the right side. Then, the left side is identical to the corresponding two-dimensional system in the X,Z plane. The equations in reference plane characteristic form (ref. 6) may be written:

Along

$$\lambda^{\pm} = \frac{dz}{dx} = \frac{M^2 \cos\phi \sin\phi \pm \beta}{M^2 \cos^2(\phi) - 1} \tag{3}$$

where $M^2 = \left(u^2 + w^2\right)/a_e^2$ and $\beta^2 = M^2 - 1$

$$d\phi \pm \frac{\beta}{\Gamma M^2} d(\ln P) = F^{\pm} d\tilde{x} \tag{4}$$

where

$$F^{\pm} = (\sin\phi - \lambda^{\pm} \cos\phi)\left[(\tan\psi)_y + \frac{\tan\psi}{\Gamma}(\ln P)_y\right]$$

$$- \phi_y \tan\psi (\cos\phi + \lambda^{\pm} \sin\phi) + \left(J_2 - \lambda^{\pm} J_1\right) \tan^2\psi$$

and

$$d\tilde{x} = \frac{dx}{J_2} + J_1 \, d(\ln x)$$

Along

$$\lambda_{SL} = \frac{dz}{dx} = \tan\phi \tag{5}$$

$$d(\tan\psi) = \frac{\tan\psi}{\Gamma M^2} d(\ln P) + G \, d\tilde{x} \tag{6}$$

where

$$G = \frac{-1}{\cos \phi}\left[\frac{(\ln P)_y}{\Gamma M^2} + \tan \psi \, (\tan \psi)_y + \tan \psi \left(1 + \tan^2 \psi\right)\left(J_1 \cos \phi + J_2 \sin \phi\right)\right]$$

The flow deflection angles ϕ and ψ, velocity components u, v, and w, and streamline and characteristic orientations $\lambda^{\pm}$ are shown in figure 4. A detailed description of orientations with respect to the various reference plane systems may be found in references 5 and 6.

CALCULATIONAL PROCEDURES

Interior Point Calculation

Properties are desired at the grid point $(\bar{I},J,K)$ shown in figure 4. The allowable step size Δx is determined by satisfying the CFL condition. For BIGMAC, this requires that the intersection of the Mach cone from $(\bar{I},J,K)$ with the initial data surface falls within the numerical domain as depicted (i.e., the quadrilateral (I,J+1), (I-1,J), (I,J-1), (I+1,J)). Note that the effective numerical domain for the characteristic calculation includes the points $I + 1$ and $I - 1$ on planes $J - 1$ and $J + 1$; hence, a larger step may be taken with CHAR3D $\left(\Delta x_{CHAR3D} \approx \sqrt{2}\, \Delta x_{BIGMAC}\right)$.

BIGMAC.- The MacCormack (ref. 12) scheme, used to difference equation (1), yields

$$\bar{E}_{\bar{I},J} = E_{I,J} - 2\,\Delta x\left(F_y + G_z - \frac{h_1}{h_3}\frac{w}{u} E_z - \frac{h_2}{h_3} F_z \tan \alpha + \frac{H}{2}\right)_{I,J} \tag{7a}$$

where

$$\tan \alpha = \pm 2\left(\frac{z_{I,J\pm1} - z_{I,J}}{\Delta y_1 + \Delta y_2}\right)\left(\frac{\Delta y_1}{\Delta y_2}\right)^{\pm 1}\left(\frac{h_3}{h_2}\right)$$

$$\left.\frac{\partial f}{\partial y}\right|_{I,J} = \pm\left(\frac{f_{I,J\pm1} - f_{I,J}}{\Delta y_1 + \Delta y_2}\right)\left(\frac{\Delta y_1}{\Delta y_2}\right)^{\pm 1}$$

$$\left.\frac{\partial f}{\partial z}\right|_{I,J} = \pm\left(\frac{f_{I\pm1,J} - f_{I,J}}{\Delta z_1 + \Delta z_2}\right)\left(\frac{\Delta z_1}{\Delta z_2}\right)^{\pm 1}$$

$$\Delta y_1 = y_{I,J} - y_{I,J-1} \qquad \Delta y_2 = y_{I,J+1} - y_{I,J}$$

$$\Delta z_1 = z_{I,J} - z_{I-1,J} \qquad \Delta z_2 = z_{I+1,J} - z_{I,J}$$

for any variable f and

$$E_{\bar{I},J} = \frac{1}{2}\left\{\left(\tilde{E}_{\bar{I},J} + E_{I,J}\right) - 2\,\Delta x\left[\tilde{F}_y + \tilde{G}_z - \frac{h_1}{h_3}\left(\frac{w}{u}\right)\tilde{E}_z - \frac{h_2}{h_3}\tilde{F}_z \tan\tilde{\alpha} + \frac{\tilde{H}}{2}\right]_{\bar{I},J}\right\} \tag{7b}$$

where

$$\tan\tilde{\alpha} = \mp 2\left(\frac{\tilde{z}_{I,J\mp1} - \tilde{z}_{I,J}}{\Delta y_1 + \Delta y_2}\right)\left(\frac{\Delta y_2}{\Delta y_1}\right)^{\pm 1}\left(\frac{h_3}{h_2}\right)$$

$$\left.\frac{\partial\tilde{f}}{\partial y}\right|_{\bar{I},J} = \mp\left(\frac{\tilde{f}_{I,J\mp1} - \tilde{f}_{I,J}}{\Delta y_1 + \Delta y_2}\right)\left(\frac{\Delta y_2}{\Delta y_1}\right)^{\pm 1}$$

$$\left.\frac{\partial\tilde{f}}{\partial z}\right|_{\bar{I},J} = \mp\left(\frac{\tilde{f}_{I\mp1,J} - \tilde{f}_{I,J}}{\Delta\tilde{z}_1 + \Delta\tilde{z}_2}\right)\left(\frac{\Delta\tilde{z}_2}{\Delta z_1}\right)^{\pm 1}$$

$$\tilde{z}_{\bar{I},J} = z_{I,J} + \left(\frac{h_1}{h_3}\frac{w}{u}\right)_{I,J}\Delta x$$

$$z_{\bar{I},J} = z_{I,J} + \frac{1}{2}\left[\left(\frac{h_1}{h_3}\frac{w}{u}\right)_{I,J} + \left(\frac{\tilde{h_1}}{h_3}\frac{w}{u}\right)_{\bar{I},J}\right]\Delta x$$

The physical variables are obtained by the following iterative procedure. A value of u is assumed. Then,

$$\rho = E(1)/u \tag{8a}$$

$$P = E(2) - E(1)\,u \tag{8b}$$

$$v = E(3)/E(1) \tag{8c}$$

$$w = E(4)/E(1) \tag{8d}$$

$$H = E(5)/E(1) \tag{8e}$$

$$\Phi = E(6)/E(1) \tag{8f}$$

$$h = H - \frac{1}{2}(u^2 + v^2 + w^2) \tag{8g}$$

The following three parameter curve fits (based on data from ref. 13) are incorporated into this code and are described in detail in the appendix of reference 6.

$$h = h(P,\Phi,T) \tag{9a}$$

$$\rho = \rho(P,\Phi,T) \tag{9b}$$

$$\Gamma = \Gamma(P,\Phi,T) \tag{9c}$$

The value of h obtained in equation (8g) yields T via an inversion of equation (9a). Equation (9b) yields an alternate value of the density compared to that obtained in equation 8(a). The value of u is perturbed and the procedure repeated until the two values of density agree to within a specified tolerance.

CHAR3D.- Point $\bar{I}$ in figure 5 is located along the quasi-streamline by the relation

$$z_{\bar{I},J} = z_{I,J} + \left(a \tan \phi_{I,J} + b \tan \phi_{\bar{I},J}\right) \Delta x$$

where $a = 1$, $b = 0$ in the predictor step and $a = \frac{1}{2}$, $b = \frac{1}{2}$ in the corrector step. In this new wave preserving network, the calculation proceeds upward from the lower boundary where points $(\bar{I}-1,J)$ are calculated for all reference planes J to second order prior to calculating points $(\bar{I},J)$. In addition to the standard initial data array (the points (I,J)), an extra array $(\hat{I},J)$ is required. To calculate properties at $(\bar{I},J)$, the standard initial data grid in the reference plane $(I-1,J)$, (I,J), and $(I+1,J)$ is employed to calculate the forcing function terms involving derivatives normal to the reference planes. Properties are known at points H_1, G_1, and $\bar{I}-1$ from the calculation of point $(\bar{I}-1,J)$ to second order.

Point A is located between H_1 and G_1 on the quasi-characteristic $\lambda^+(A\bar{I})$ where $\lambda^{\pm}$ is defined in equation (3). All properties (including forcing functions) are

obtained via linear interpolation[1] between H_1 and G_1. Then, H_2 is located between $\hat{I}$ and $I+1$ such that the downrunning quasi-characteristic from G_2 (or B) passes through $(\bar{I},J)$. To first order, properties at $(\bar{I},J)$ are calculated using points B and A, where P_B and ϕ_B are determined using compatibility relations (eq. (4)) along IB and H_2B.

Then $P_{\bar{I}}$ and $\phi_{\bar{I}}$ are calculated employing the compatibility relations

$$\left.\begin{aligned}
&(\phi_{\bar{I}} - \phi_A) + \left[a\left(\frac{\beta}{\Gamma M^2}\right)_A + b\left(\frac{\beta}{\Gamma M^2}\right)_{\bar{I}}\right] \ln\left(\frac{P_{\bar{I}}}{P_A}\right) = \left(aF_A^+ + bF_{\bar{I}}^+\right)\Delta\tilde{x}_{\bar{I}A} \\
&\text{and} \\
&(\phi_{\bar{I}} - \phi_B) - \left[a\left(\frac{\beta}{\Gamma M^2}\right)_B + b\left(\frac{\beta}{\Gamma M^2}\right)_{\bar{I}}\right] \ln\left(\frac{P_{\bar{I}}}{P_B}\right) = \left(aF_B^- + bF_{\bar{I}}^-\right)\Delta\tilde{x}_{\bar{I}B}
\end{aligned}\right\} \quad (10)$$

Remaining properties are determined at $\bar{I}$ via the following streamline relations:

$$(\tan\psi)_{\bar{I}} = (\tan\psi)_{\bar{I}} + \left[a\left(\frac{\tan\psi}{\Gamma M^2}\right)_I + b\left(\frac{\tan\psi}{\Gamma M^2}\right)_{\bar{I}}\right] \ln\left(\frac{P_{\bar{I}}}{P_I}\right) + \left(aG_I + bG_{\bar{I}}\right)\Delta\tilde{x}_{I\bar{I}} \quad (11)$$

$$H_{\bar{I}} = H_I - \left[a\left(\frac{\tan\psi}{\cos\phi}H_y\right)_I + b\left(\frac{\tan\psi}{\cos\phi}H_y\right)_{\bar{I}}\right]\Delta\tilde{x}_{I\bar{I}} \quad (12)$$

$$\phi_{\bar{I}} = \phi_I - \left[a\left(\frac{\tan\psi}{\cos\phi}\Phi_y\right)_I + b\left(\frac{\tan\psi}{\cos\phi}\Phi_y\right)_{\bar{I}}\right]\Delta\tilde{x}_{I\bar{I}} \quad (13)$$

and in continuous regions of the flow

$$\left(P/\rho\Gamma\right)_{\bar{I}} = \left(P/\rho\Gamma\right)_I - \left\{a\left[\frac{\tan\psi}{\cos\phi}\left(P/\rho\Gamma\right)_y\right]_I + b\left[\frac{\tan\psi}{\cos\phi}\left(P/\rho\Gamma\right)_y\right]_{\bar{I}}\right\}\Delta x_{I\bar{I}} \quad (14)$$

---

[1]Linear interpolation along a characteristic line calculated to second order is consistent to second order. (See appendix.)

The flow velocity is obtained via the relation

$$V_{\bar{I}} = \sqrt{2}\left[H_{\bar{I}} - h\left(P_{\bar{I}}, \Phi_{\bar{I}}, T_{\bar{I}}\right)\right]^{1/2} \tag{15}$$

where $T_{\bar{I}}$ is obtained via an inversion of equation (9b) (with $\rho_{\bar{I}}$, $P_{\bar{I}}$, and $\Phi_{\bar{I}}$ known) and $h_{\bar{I}}$ is obtained employing equation (9a). Then, $\Gamma_{\bar{I}}$ is obtained from equation (9c) and $a_e^2 = \Gamma_{\bar{I}} P_{\bar{I}}/\rho_{\bar{I}}$.

This calculation is performed for points $\bar{I}$ in <u>all</u> reference planes to first order. Then, cross derivatives $\partial/\partial y$ are evaluated at $\bar{I}$ employing the relation

$$\left(\frac{\partial f}{\partial y}\right)_{x,z} = \left(\frac{\partial f}{\partial y}\right)_{x,\eta} - \tan\alpha \left(\frac{\partial f}{\partial z}\right)_{x,y} \tag{16}$$

where

$$\left(\frac{\partial f}{\partial y}\right)_{x,\eta} = \frac{f_{\bar{I},J+1}\left(\frac{\Delta y_1}{\Delta y_2}\right) + f_{\bar{I},J}\left(\frac{\Delta y_2}{\Delta y_1} - \frac{\Delta y_1}{\Delta y_2}\right) - f_{\bar{I},J-1}\left(\frac{\Delta y_2}{\Delta y_1}\right)}{(\Delta y_1 + \Delta y_2)}$$

$$\Delta y_1 = y_{\bar{I},J} - y_{\bar{I},J-1} \qquad \Delta y_2 = y_{\bar{I},J+1} - y_{\bar{I},J}$$

$$\tan\alpha = \left(\frac{\partial z}{\partial y}\right)_{x,\eta}$$

$$\left(\frac{\partial f}{\partial z}\right)_{x,y} = \frac{f_{\bar{I},J} - f_{\bar{I}-1,J}}{z_{\bar{I},J} - z_{\bar{I}-1,J}}$$

Derivatives are made the same way at the initial station I, except here $\partial f/\partial z$ is evaluated by

$$\left(\frac{\partial f}{\partial z}\right)_{x,y} = \frac{f_{I+1,J} - f_{I,J}}{z_{I+1,J} - z_{I,J}}$$

CHAR3D, in addition to the centered difference algorithm described above, has the option of evaluating cross derivatives via an alternating one-sided difference algorithm. For this option, derivatives are evaluated as described in the section for BIGMAC. Cross

derivatives are required for the variables P, ϕ, ψ, H, Φ, and P/ρ^{Γ}. In evaluating cross derivatives for P, ϕ, and ψ, conservation variables are employed as follows:

$$\left.\begin{aligned} P_y &= F(3)_y - F(1)\, v_y - v\, F(1)_y \\ \phi_y &= \frac{w_y \cos\phi - u_y \sin\phi}{q} \\ (\tan\psi)_y &= \frac{q v_y - (u u_y + w w_y)\tan\psi}{q^2} \end{aligned}\right\} \tag{17}$$

where

$$u = q\cos\phi \qquad w = q\sin\phi \qquad v = q\tan\psi$$

$$q^2 = u^2 + w^2$$

and

$$\left.\begin{aligned} v_y &= \frac{E(3)_y - v\, E(1)_y}{E(1)} \\ u_y &= \frac{E(2)_y - h_2 h_3 P_y - u\, E(1)_y}{E(1)} \\ w_y &= \frac{E(4)_y - w\, E(1)_y}{E(1)} \end{aligned}\right\} \tag{18}$$

The conservation variables $E(k)$ and $F(k)$ are given by equation (1). The use of conservation variables in construction of these cross derivatives tends to suppress oscillations that occur when employing physical variables to difference across shock waves. However, the use of a one-sided difference algorithm in conjunction with CHAR3D tends to produce spurious results in regions of large cross flow.

In the characteristic reference plane algorithm, cross flow variations are expressed via the forcing function terms $F^{\pm}$ appearing in the right side of the compatibility relations (eq. (4)). These terms are assumed to vary mildly within an integration step. When a one-sided algorithm is employed to evaluate cross derivatives in the vicinity of shocks, the values of the forcing function terms may vary greatly between the predictor and corrector steps. In addition, the numerical domain of dependence is somewhat vague for the characteristic reference plane approach in conjunction with one-sided differences, so that

part of the problem may be due to stability. The recommended approach for evaluating cross derivatives in CHAR3D is to employ conservation variables in conjunction with a centered difference algorithm, although this matter requires further study.

In CHAR3D, secondary shocks are captured as rapid changes spread over approximately three grid points. These discontinuities are preserved by use of the wave network described which performs all interpolations off quasi-characteristic surfaces. The entropy change associated with these shocks is evaluated employing a nonisentropic pressure-density relation (illustrated here for a perfect gas)

$$\vec{V} \cdot \nabla \ln \left(P/\rho^{\Gamma}\right) = \vec{V} \cdot \frac{\nabla S}{C_v} \tag{19}$$

For a shock of strength ξ (pressure ratio across shock), this change is determined employing the relation (for perfect gas)

$$\frac{\Delta S}{C_v} = \ln \xi - \Gamma \ln \left[\frac{(\Gamma + 1)\xi + (\Gamma - 1)}{(\Gamma - 1)\xi + (\Gamma + 1)}\right] \tag{20}$$

where ΔS is the entropy change along a streamline produced by the captured shock. This relation involves only the pressure distribution in the vicinity of the shock and is readily applied in regions of noninteracting shocks as follows. Let

$$F(\xi,\Gamma) = \frac{(\Gamma + 1)\xi + (\Gamma - 1)}{(\Gamma - 1)\xi + (\Gamma + 1)}$$

Assume a shock is spread over the marching interval $K = 1$ to 6 (fig. 6) for a typical quasi-streamline. Then 1 represents free stream conditions for this shock. The entropy change in the interval $K - 1$ to K is then expressed by

$$\left(\frac{\Delta S}{C_v}\right)_{K-1,K} = \left(\frac{\Delta S}{C_v}\right)_{1,K} - \left(\frac{\Delta S}{C_v}\right)_{1,K-1} = \ln \left[\frac{\xi_{1,K}}{\xi_{1,K-1}} \left(\frac{F_{1,K-1}}{F_{1,K}}\right)^{\Gamma}\right]$$

where

$$\xi_{1,K} = P_K/P_1$$

Then

$$\left(P/\rho^{\Gamma}\right)_K = \left[\left(P/\rho^{\Gamma}\right)_{K-1} - \frac{\tan \psi}{\cos \phi} \left(P/\rho^{\Gamma}\right)_y \Delta\tilde{x}_{K-1,K}\right] \exp \left(\frac{\Delta S}{C_v}\right)_{K-1,K}$$

Since the shock geometry does not appear in the entropy jump relation, the entropy rise associated with extremely complex three-dimensional shocks can be accurately obtained. Special provisions have been incorporated into the program for the computation of singular points at the juncture of intersecting shock waves and/or shock reflection points. At such points the streamline undergoes a discontinuous pressure rise corresponding to that through both shock waves. If the shock intensities are different, an entropy discontinuity occurs separating the different zones, and a vortex of infinite intensity results. Numerically, the entropy procedure described would predict an entropy rise associated with this pressure jump. Theoretically, this occurs in the limit of vanishing mass flow, while numerically the finite mass within this region would lead to unduly large entropy levels. Special coding has been incorporated at such singular points to suppress these "numerical" peaks.

Wall Point Calculation

Solid surfaces are prescribed via discrete contour data and fitted via a newly developed method based on the use of partial cubic splines (ref. 14). The surface fitting is done by a separate geometry package and the array of coefficients generated is stored on tape. BIGMAC and CHAR3D employ this coefficient data in conjunction with a surface interpolation procedure yielding highly accurate values of the dependent variable and surface unit normal.

In both BIGMAC and CHAR3D, wall point calculations are performed employing a reference plane characteristic calculation. In figure 7, CD is the intersection of the reference plane $y = y_C$ with the surface $z = f(x,y)$. Reference planes are oriented so that the surface normal lies nearly within the reference plane. For sidewall calculations, this is accomplished via local coordinate rotations.

In CHAR3D, P_C, ϕ_C, and ψ_C are evaluated utilizing the characteristic compatibility relation (eq. (4)) along BC, the normal momentum equation (eq. (6)) along the streamline projection CD^*, and the relation $\vec{V} \cdot \hat{n} = 0$ applied at C, which yield the relation

$$\sin \phi_C = (f_x)_C \cos \phi_C + (f_y)_C \tan \psi_C \tag{21}$$

The compatibility equation yields a relation between P_C and ϕ_C, and the normal momentum equation yields a relation between P_C and ψ_C. This system is solved in the context of the wave preserving network previously described by a simple iterative procedure.

In BIGMAC, this iterative procedure is eliminated by combining the normal momentum equation with the quasi-streamline momentum equation, yielding the following system of equations for P_C, $(w/u)_C$, and $(v/u)_C$:

$$\begin{vmatrix} (\rho u^2/\beta P)_{BC} & \pm 1 & 0 \\ 1 & 0 & -(f_y)_C \\ (\tan\psi \sin\phi)_{CD^*} & \left(\frac{P \tan\psi \cos\phi}{\rho u^2}\right)_{CD^*} & -1 \end{vmatrix} \begin{vmatrix} (w/u)_C \\ \ln P_C \\ (v/u)_C \end{vmatrix} = \begin{vmatrix} R_1 \\ R_2 \\ R_3 \end{vmatrix} \qquad (22)$$

where

$$R_1 = -\frac{1}{\beta P h_1 h_2 h_3}\left[(\lambda^{\pm} u - w)A - \lambda^{\pm} B + C\right]_{BC} \Delta x \pm \ln P_B + \left(\frac{\rho u^2}{\beta P}\right)_{BC}\left(\frac{w}{u}\right)_B$$

$$R_2 = (f_x)_C$$

$$R_3 = \frac{1}{\rho u^2 h_1 h_2 h_3}\left[E_{SL} - \tan\psi\,(B\cos\phi + C\sin\phi)\right]_{CD^*} \Delta x$$

and

$$A = h_1 h_3\left(\frac{v P_y}{a_e^2} + \rho v_y\right) + J_1 \frac{E(1)}{h_2} + J_2 \frac{G(1)}{h_2}$$

$$B = F(2)_y - u\,F(1)_y - J_1 \frac{v\,F(1)}{h_1}$$

$$C = F(4)_y - w\,F(1)_y - J_2 \frac{v\,F(1)}{h_3}$$

$$E_{SL} = F(3)_y - v\,F(1)_y + J_1 \frac{F(2)}{h_1} + J_2 \frac{F(4)}{h_3}$$

Then, relations applied along the streamline projection CD^* yield remaining flow variables at C, in conjunction with the equilibrium curve fits (eq. (9)), for both programs. The process is then repeated with coefficients averaged for second order accuracy.

Interior Corner

Interior corners occur in the internal modules and are discretely treated as the intersection of specified surfaces, as depicted in figure 8. A detailed description of these corner calculations with respect to the various reference plane coordinate systems may be found in reference 6. The procedure is outlined here for a Cartesian system where the intersecting surfaces are prescribed by $z = f(x,y)$ and $y = g(x,z)$.

The relation $\vec{V} \cdot \hat{n} = 0$ applied to both intersecting surfaces at C (the point to be calculated) yields the flow deflection angles ϕ_C and ψ_C explicitly

$$\left.\begin{aligned} \phi_C &= \tan^{-1}\left(\frac{f_x + g_x f_y}{1 - g_z f_y}\right) \\ \psi_C &= \tan^{-1}\left(\cos\phi_C \frac{g_x + f_x g_z}{1 - f_y g_z}\right) \end{aligned}\right\} \tag{23}$$

Then, a redundant procedure is employed wherein reference plane calculations for the pressure at C are performed in the reference planes $z = z_C$ and $y = y_C$. This yields two values of pressure P_{C_1} and P_{C_2} which differ due to evaluating the cross derivative forcing function terms in the compatibility relations via backward differences. A weighting of these pressures is performed by accounting for the relative wave strengths in each of these reference planes. This gives the stronger weighting to the calculation performed in the reference plane containing the dominant waves via the relation

$$P_C = \frac{\Delta\psi_{A_1C}}{\Delta\psi_{A_1C} + \Delta\phi_{A_2C}} P_{C_1} + \frac{\Delta\phi_{A_2C}}{\Delta\psi_{A_1C} + \Delta\phi_{A_2C}} P_{C_2} \tag{24}$$

Streamline relations are performed along the corner CD, and the process is repeated for second order accuracy.

Shock Point Calculation

A discrete three-dimensional shock point calculation is performed for the nozzle underexpansion shock, which propagates into the nonuniform external stream surrounding the vehicle. In figure 9, subscript 2 refers to the shock free stream. Shock geometry is defined in terms of the direction cosines of α and β, where β is the angle made by the shock cut with the reference plane and α is the crosscut angle. For given values of α and β, the shock normal is

$$\hat{n}_s = \hat{i}_x \cos\alpha \sin\beta - \hat{i}_y \sin\alpha + \hat{i}_z \cos\alpha \cos\beta \tag{25}$$

where $\hat{i}_x, \hat{i}_y, \hat{i}_z$ are the unit vectors in the x-, y-, and z-directions. The characteristic relations on the free stream side yield flow properties at C_2. The Hugoniot relations in a shock normal system yield properties at C_1. The compatibility relation along A_1C_1 yields an alternate value of pressure $P^*_{C_1}$. The angle β is perturbed locally until P_{C_1} from the jump relations equals $P^*_{C_1}$ from the compatibility relations to within a specified tolerance. This procedure is performed in all reference planes, and the process is then repeated using updated values of the crosscut angle α. The complete details of this procedure including rotation into the shock oriented system, jump relations, and iterative procedures may be found in references 5 and 6.

Contact Surface Calculation

A three-dimensional contact surface is significantly more complex than its two-dimensional counterpart, since the streamlines on each side of the discontinuity not only differ in velocity magnitude but also may be highly skewed with respect to each other. In figure 10, α and β are as previously defined for the shock calculation, and the streamlines passing through C emanate from D_1 on the lower side and D_2 on the upper side. Hence, discontinuities exist in the flow angles ϕ and ψ at point C. The boundary relation $\vec{V} \cdot \hat{n} = 0$ applied at C_1 and C_2 yields the relations

$$\left.\begin{aligned} \sin\left(\beta - \phi_{C_1}\right) + \tan\alpha \tan\psi_{C_1} = 0 \\ \sin\left(\beta - \phi_{C_2}\right) + \tan\alpha \tan\psi_{C_2} = 0 \end{aligned}\right\} \tag{26}$$

Then, characteristic compatibility relations may be applied along A_1C_1 and B_2C_2 yielding $P_{C_1} - \phi_{C_1}$ and $P_{C_2} - \phi_{C_2}$ relations. The normal momentum relations applied along the streamline projections $C_1D_1^*$ and $C_2D_2^*$ yield relations between $P_{C_1} - \psi_{C_1}$ and $P_{C_2} - \psi_{C_2}$. For a given value of the crosscut angle α, a value of β is obtained via an iterative process satisfying the above relations and the boundary condition $P_{C_1} = P_{C_2}$. This procedure is performed in all reference planes and repeated with updated values of the crosscut angle α. Again, complete details may be found in references 5 and 6.

RESULTS

Internal corners represent just one segment of the overall boundary calculational procedure and hence must be calculated as part of the overall marching procedure.

Recently, inviscid corner flow fields have been studied in detail (refs. 15 and 16) utilizing conical coordinates in a timelike marching procedure until conical invariance was achieved. While these schemes do yield the flow field details in the corner region, they are not applicable to general three-dimensional flow problems which are nonconical.

Corner results are presented using the general interior corner point calculation outlined above and previously described in references 5 and 6. Results for a 5° double expansion corner are depicted in figures 11 and 12. These results were obtained with CHAR3D starting from uniform initial flow conditions $\left(P_{\infty} = 845,\ M_{\infty} = 2.94,\ \phi = \psi = 0\right)$ with an 11×11 Cartesian grid. Results are shown after nine axial marching steps and the axial pressure variation at the corner is also indicated. Similar results have been obtained with BIGMAC.

An expansion-compression has been calculated using BIGMAC which yielded the results depicted in figure 13. These results were obtained with an 11×11 Cartesian grid for initially uniform flow $\left(M_{\infty} = 2\right)$ and are depicted after 10 axial marching steps. Results are compared with the detailed solution of Shankar (ref. 16) and the experimental results of Nangia (ref. 17).

Results for the double compression corner, as obtained by BIGMAC, are shown in figure 14 after 35 axial marching steps. A 12×12 line source network was employed with initially uniform flow at $M_{\infty} = 3.17$. A comparison is made with Shankar's numerical results (ref. 16) and the experimental results of Charwat and Redekeopp (ref. 18).

The above results verify the accuracy and validity of the interior corner procedure employed and, hence, yield credibility to the application of this procedure for general corner calculations within "truly" three-dimensional flow fields.

To demonstrate results obtainable with the new wave preserving network of CHAR3D, a simple two-dimensional inlet flow field is calculated. Calculation was performed with a uniform equally spaced initial profile ($P = 845$, $M = 2.94$) employing 11 and 21 grid points. Wall pressures are depicted in figures 15 and 16 for three shock reflections. After the fourth reflection, the flow on the upper boundary is subsonic, and thus the program could not calculate past this region. Note that both the pressures obtained as well as the propagation rates are in excellent agreement with the exact solution and no additional smearing results from wall reflections.

A complex internal module flow field calculation (square nozzle) as depicted in figure 17 has been performed using BIGMAC. This flow field is characterized by the initial interactions of expansion waves emanating from mutually perpendicular surfaces and the subsequent interaction of enveloping shock systems generated by recompression on the upper wall and sidewall. This calculation employed a 21×11 Cartesian network, with

additional reference planes being inserted as the sidewall opened. At the straight section the final network was 21×18. Uniform flow properties $(P_\infty = 845, \ M_\infty = 2.94)$ were stipulated at the nozzle entrance. Pressure contours on the symmetry plane are depicted in figure 18. Of particular interest is the intersection of four three-dimensional shock surfaces at $x \approx 17$ and $z = y = 0$. This results from the reflection of the envelope shock produced by the sidewall and the reflection of the envelope shock produced by the upper wall, resulting in an approximate 15/1 pressure ratio at this location. The axial pressure variation along the corner is depicted in figure 19 and pressure variations along several streamlines in the symmetry plane are depicted in figure 20.

All results presented employed a perfect gas option with $\Gamma = 1.4$ for the sake of simplicity. The equilibrium option has been extensively used and tested (refs. 5, 6, 7, and 8) and provides no further insight into these problems. The results were all obtained with relatively crude grid networks, yet provided accurate and detailed flow field results. Further grid refinement would yield somewhat better flow resolution, if desired or necessary. It should be noted that due to the use of disc storage techniques, as employed in both programs, flow field resolution is not limited by machine core storage.

CONCLUDING REMARKS

Two new computer codes have been developed for analyzing complex three-dimensional supersonic flow fields. Their use of a quasi-streamline network in conjunction with a reference plane grid allows for the calculation of complex geometric configurations and caters to highly rotational, variable composition flow fields. Both BIGMAC and CHAR3D are currently running internal flow codes with perfect gas or equilibrium hydrogen-air chemistry options.

CHAR3D employs a totally new grid network which caters to both the following of streamlines and the preservation of wave systems. This is done in conjunction with an axial marching procedure. Hence, in addition to its application to three-dimensional reference plane systems, it is equally applicable to "viscous" characteristic techniques, since forcing functions are also employed.

BIGMAC employs the commonly used MacCormack algorithm in conjunction with conservation variables and hence falls in the general classification of finite difference shock capturing codes. However, it does this in conjunction with a reference plane streamline grid which provides significant advantages for the flow fields treated.

Both programs treat complex three-dimensional flow fields accurately, locating secondary shock waves and evaluating flow field properties in their vicinity including wall and interior flow entropy. From our limited experience with these codes, CHAR3D appears best suited to flow fields wherein the predominant wave propagation occurs within

the reference planes. For such flow fields, CHAR3D with half the grid points yields results comparable to those of BIGMAC. In addition, no overshoots occur in the vicinity of shock waves and a larger marching step may be taken. However, when the assumption of a mildly varying forcing function is violated (i.e., in the vicinity of strong crosswise compressions) BIGMAC would be the preferred code. This program has no preferential direction and has been shown capable of calculating arbitrary multishocked three-dimensional flow fields.

Our current effort is devoted to extending both these codes for the calculation of the flow field downstream of the engine modules. This calculation is performed in the authors' previous code and similar procedures will be incorporated. Future efforts will involve the incorporation of finite-rate hydrogen-air chemistry, frozen chemistry, and associated sudden freezing criterion. In addition, the extension of these codes to mixing calculations along the plume interface is anticipated.

It should be noted that while the calculation of nozzle exhaust flow fields has been specifically discussed, both codes are capable of analyzing quite general three-dimensional flow fields. Results to date indicate that these techniques yield minimum smearing of captured shocks, even after multiple reflections and/or intersections. Thus, these codes appear capable of calculating inlet type flow fields and can readily be modified to calculate the simpler problem of external supersonic flows.

APPENDIX

LINEAR INTERPOLATION ON CHARACTERISTIC

A SECOND ORDER PROCEDURE

In previous reference plane characteristic codes (employing inverse interpolation procedures), data are interpolated on a noncharacteristic surface. To achieve full second order accuracy, most codes resort to higher order interpolation procedures. Such procedures are helpful in smooth regions of the flow field but are detrimental in regions of weak discontinuities. In such regions, linear interpolation is more accurate as explicitly discussed by Sedney (ref. 1). The authors had performed an independent study (unpublished) on such higher order interpolation procedures and concluded that for general multiwave flow fields, linear interpolations provide the most accurate results.

Now, with this new "wave preserving" network, all interpolations are performed on characteristic lines. Employing a linear interpolation procedure on a characteristic line calculated to second order is consistent with a second order algorithm. This point can be inferred from Ferri's article (ref. 19) but apparently, is not universally accepted. (See ref. 1.) Hence, a simple proof of this statement is presented.

Along any line AC, a series expansion for the pressure and flow deflection are written

$$P_C = P_A + (P_x)_A \Delta x + (P_{xx})_A (\Delta x)^2/2 + 0\,(\Delta x)^3 \tag{A1}$$

$$\phi_C = \phi_A + (\phi_x)_A \Delta x + (\phi_{xx})_A (\Delta x)^2/2 + 0\,(\Delta x)^3 \tag{A2}$$

but

$$(P_x)_C = (P_x)_A + (P_{xx})_A \Delta x + 0\,(\Delta x)^2 \tag{A3}$$

$$(\phi_x)_C = (\phi_x)_A + (\phi_{xx})_A \Delta x + 0\,(\Delta x)^2 \tag{A4}$$

where x denotes distance along AC.

Substituting equation (A3) into equation (A1) and equation (A4) into equation (A2) results in

$$P_C = P_A + \left[(P_x)_A + (P_x)_C\right](\Delta x/2) + 0\,(\Delta x)^3 \tag{A5}$$

$$\phi_C = \phi_A + \left[(\phi_x)_A + (\phi_x)_C\right](\Delta x/2) + 0\,(\Delta x)^3 \tag{A6}$$

The previous expressions are valid along any line AC. Assuming that AC is a down-running characteristic, the compatibility relations at points A and C are

$$(\phi_x)_A - A_A(P_x)_A = 0 \tag{A7}$$

$$(\phi_x)_C - A_C(P_x)_C = 0 \tag{A8}$$

where

$$A = \frac{\beta}{\Gamma M^2 P}$$

Solving the system of equations (A5) to (A8) for $(P_x)_A + (P_x)_C$ results in

$$(P_x)_A = \frac{-2}{\Delta x(A_C - A_A)}\left[(\phi_C - \phi_A) - A_C(P_C - P_A)\right] \tag{A9}$$

and

$$(P_x)_C = \frac{2}{\Delta x(A_C - A_A)}\left[(\phi_C - \phi_A) - A_A(P_C - P_A)\right] \tag{A10}$$

Now consider a point x^* between A and C. The pressure at this point to second order is given by

$$P^* = P_A + (P_x)_A(x^* - x_A) + \frac{(P_x)_C - (P_x)_A}{\Delta x_{AC}}(x^* - x_A)^2 + 0\,(\Delta x)^3 \tag{A11}$$

where $(P_x)_A$ and $(P_x)_C$ are given by equations (A9) and (A10). Up to this point, all relations are quite general and have not required that a second order compatibility relation exist between A and C. We now make use of this relation by stating that by second order, we imply that the relation

$$(\phi_C - \phi_A) - \left(\frac{A_A + A_C}{2}\right)(P_C - P_A) = 0 \tag{A12}$$

is satisfied between points A and C in a convergent fashion as detailed in reference 19. Then, substituting equation (A12) into equations (A9) and (A10) results in

$$(P_x)_C - (P_x)_A = 0 \tag{A13}$$

and

$$(P_x)_A = \frac{P_C - P_A}{x_C - x_A} \tag{A14}$$

Hence, substituting these relations into equation (A11) yields

$$P^* = P_A + (P_C - P_A)\left(\frac{x^* - x_A}{x_C - x_A}\right) + 0\ (\Delta x)^3$$

which clearly demonstrates that a linear interpolation for pressure (or flow deflection) on a characteristic calculated to second order is consistent with a fully second order approach.

REFERENCES

1. Sedney, R.: The Method of Characteristics. Nonequilibrium Flows, Part II, Marcel Dekker Inc., New York (1970).

2. Dash, S.: An Analysis of Internal Supersonic Flows With Diffusion, Dissipation and Hydrogen-Air Combustion. NASA CR-111783, 1970.

3. Dash, S.; and Del Guidice, P.: Analysis of Supersonic Combustion Flow Fields With Embedded Subsonic Regions. NASA CR-112223, 1972.

4. Abett, M. J.: Boundary Condition Calculational Procedures for Inviscid Supersonic Flow Fields. AIAA Computational Fluid Dynamics Conference Proceedings, July 1973.

5. Dash, S.; and Del Guidice, P.: Three Dimensional Nozzle Exhaust Flow Field Analysis by a Reference Plane Technique. AIAA Paper No. 72-704, June 1972.

6. Dash, S.; and Del Guidice, P.: Analysis and Design of Three-Dimensional Supersonic Nozzles, Vol. I. NASA CR-132350, 1972.

7. Edwards, C. L. W.; Small, W. J.; and Weidner, J. P.: Studies of Scramjet/Airframe Integration Techniques for Hypersonic Aircraft. AIAA Paper No. 75-58, Jan. 1975.

8. Small, W. J.; Weidner, J. P.; and Johnston, P. J.: Scramjet Nozzle Design and Analysis as Applied to a Highly Integrated Research Airplane. NASA TM X-71972, 1974.

9. Rakich, J. V.: Three-Dimensional Flow Calculation by the Method of Characteristics. AIAA J., vol. 5, no. 10, 1967.

10. Katskova, O. N.; and Chuskin, P. I.: Three-Dimensional Supersonic Equilibrium Flow of Gas Around Bodies at Angles of Attack. NASA TT F-9790, 1965.

11. Rakich, J. V.; and Kutler, P.: Comparison of Characteristics and Shock Capturing Methods With Application to the Space Shuttle Vehicle. AIAA Paper No. 72-191, Jan. 1972.

12. MacCormack, R. W.: The Effect of Viscosity in Hypervelocity Impact Cratering. AIAA Paper No. 69-354, 1969.

13. Barnes, B.; McIntyre, R. W.; and Sims, J. A.: Properties of Air and Combustion Products With Kerosine and Hydrogen Fuels. Published by Bristol Siddley Engines Ltd. on behalf of Group for Aerospace R&D, 1967.

14. Dash, S.; and Kalben, P.: Three-Dimensional Surface Representation and Interpolation Procedures Employing Cubic Spline Functions. ATL TR-193, Jan. 1974.

15. Kutler, P.: Supersonic Flow in the Corner Formed by Two Intersecting Wedges. AIAA J., vol. 12, no. 5, May 1974.

16. Shankar, V. S. V.: Numerical Solutions for Inviscid Supersonic Corner Flows. AIAA Paper No. 75-221, Jan. 1975.

17. Nangia, P. K.: Three-Dimensional Wave Interactions in Supersonic Intakes. 2nd Int. Symposium on Air Breathing Engines, Sheffield, England, Mar. 1974.

18. Charwat, A. F.; and Redekeopp, L. G.: Supersonic Interference Flow Along the Corner of Intersecting Wedges. AIAA J., vol. 5, no. 3, Mar. 1967.

19. Ferri, A.: The Method of Characteristics. Section G of The General Theory of High Speed Aerodynamics, Vol. VI of Princeton Series, Princeton University Press, 1954.

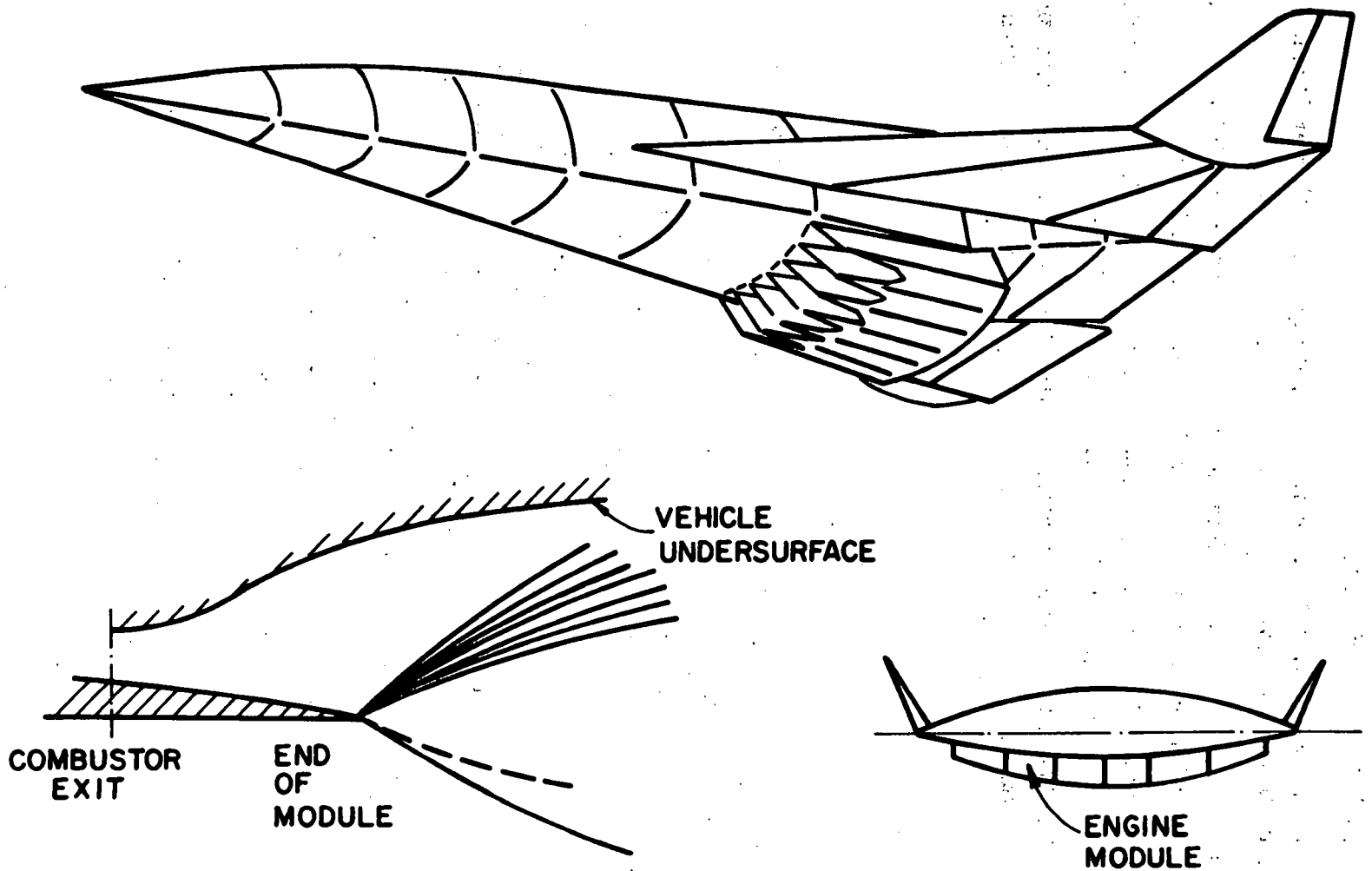

Figure 1.- Hypersonic research airplane.

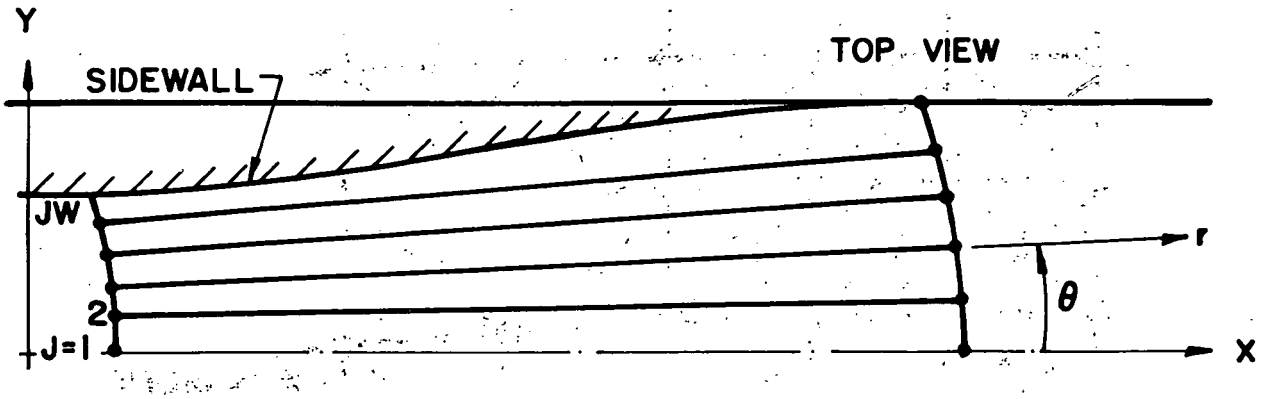

(a) In line source system for internal nozzle module. JW designates sidewall.

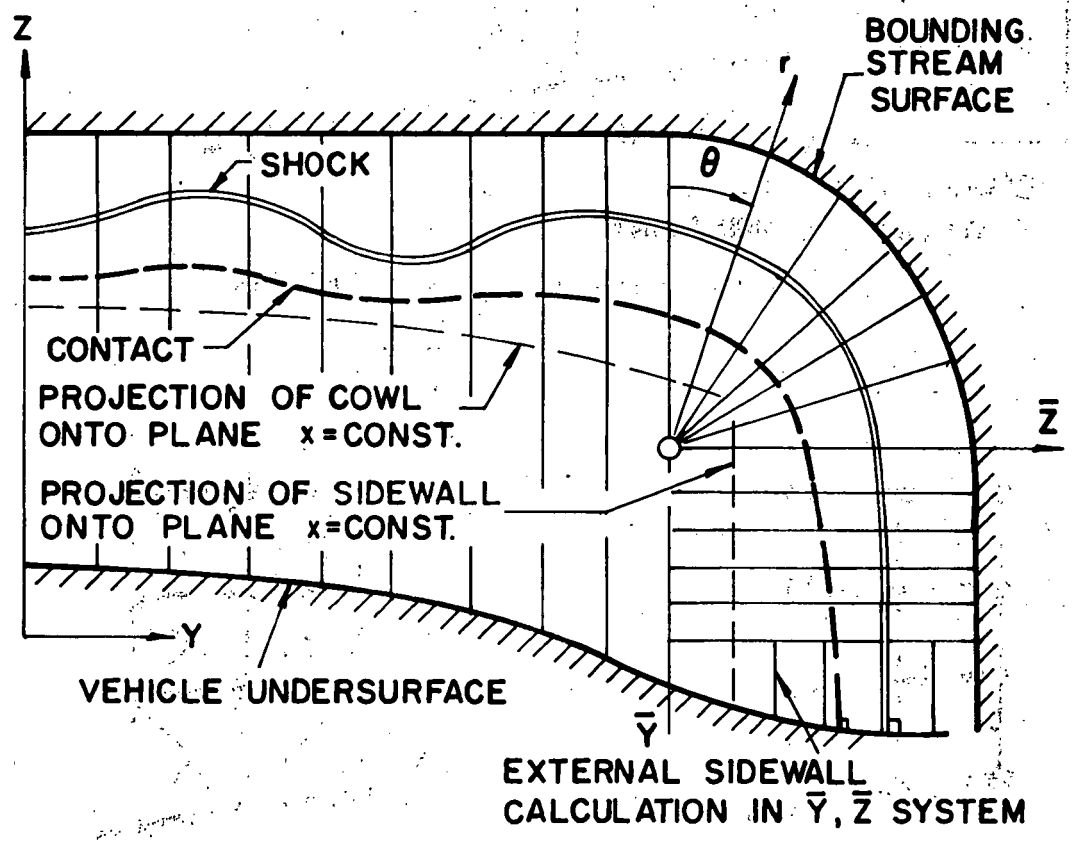

(b) Downstream of modules.

Figure 2.- Reference plane configuration.

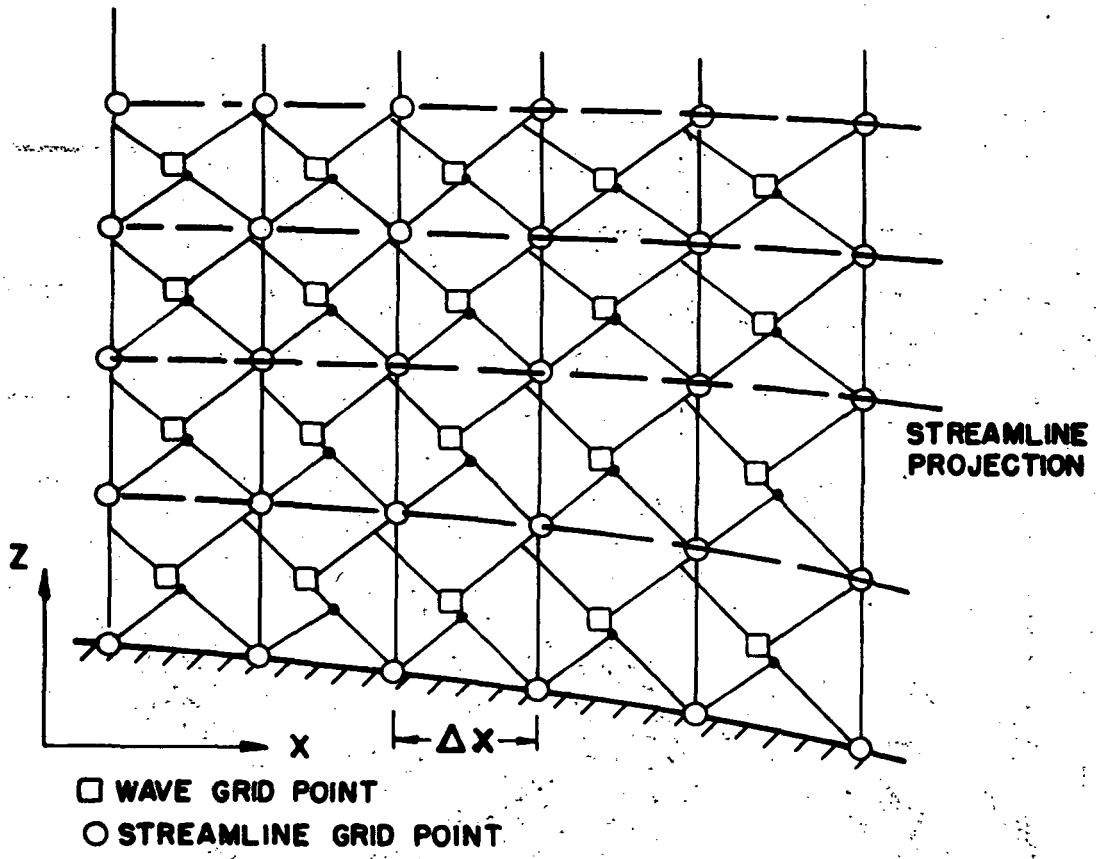

(a) Reference plane grid network for CHAR3D.

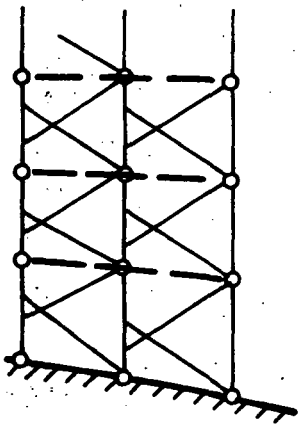

(b) Standard reference plane characteristic network.

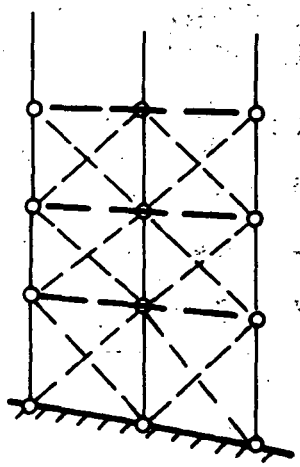

(c) Finite difference network.

Figure 3.- Reference plane networks.

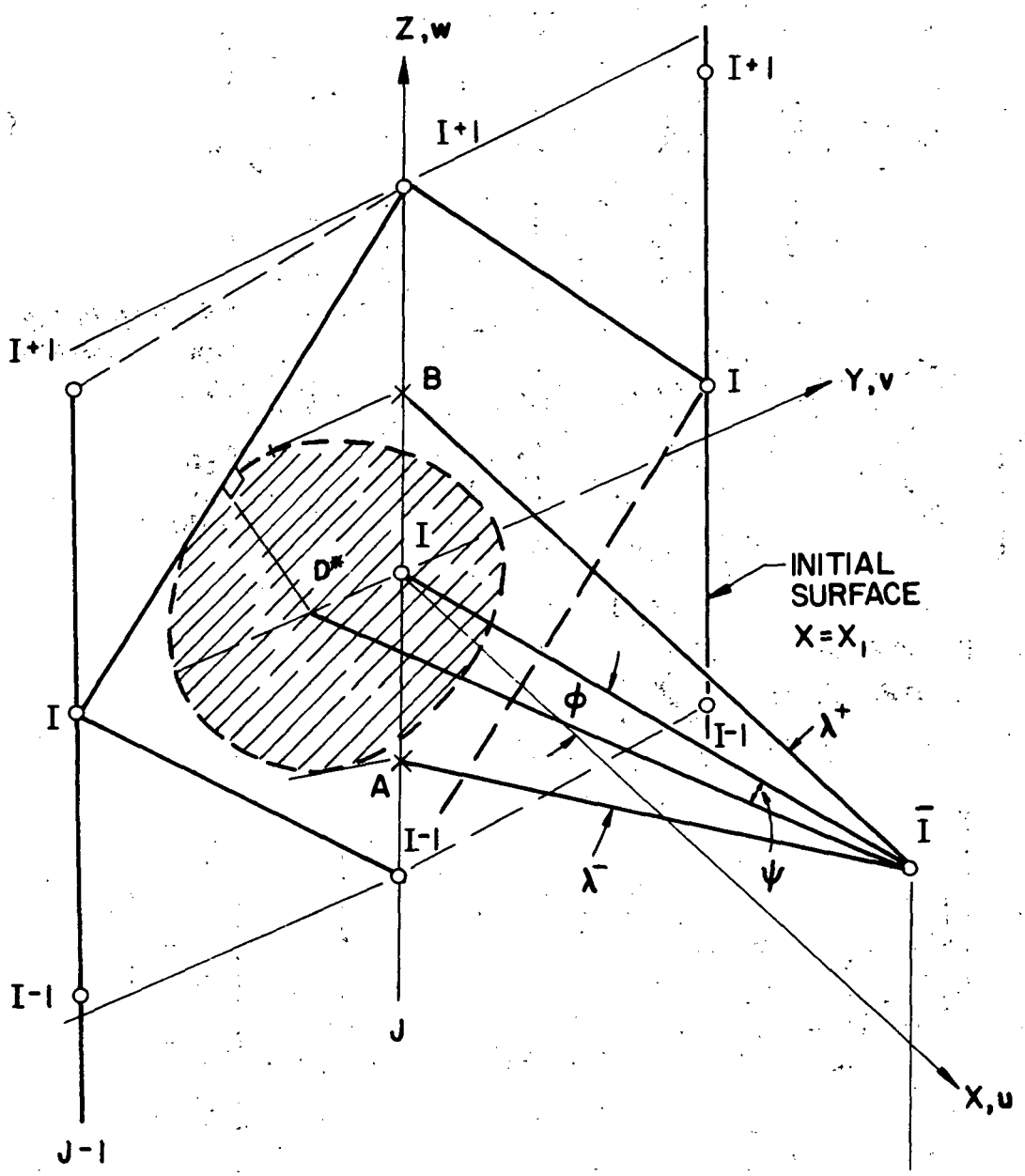

Figure 4.- Interior grid point.

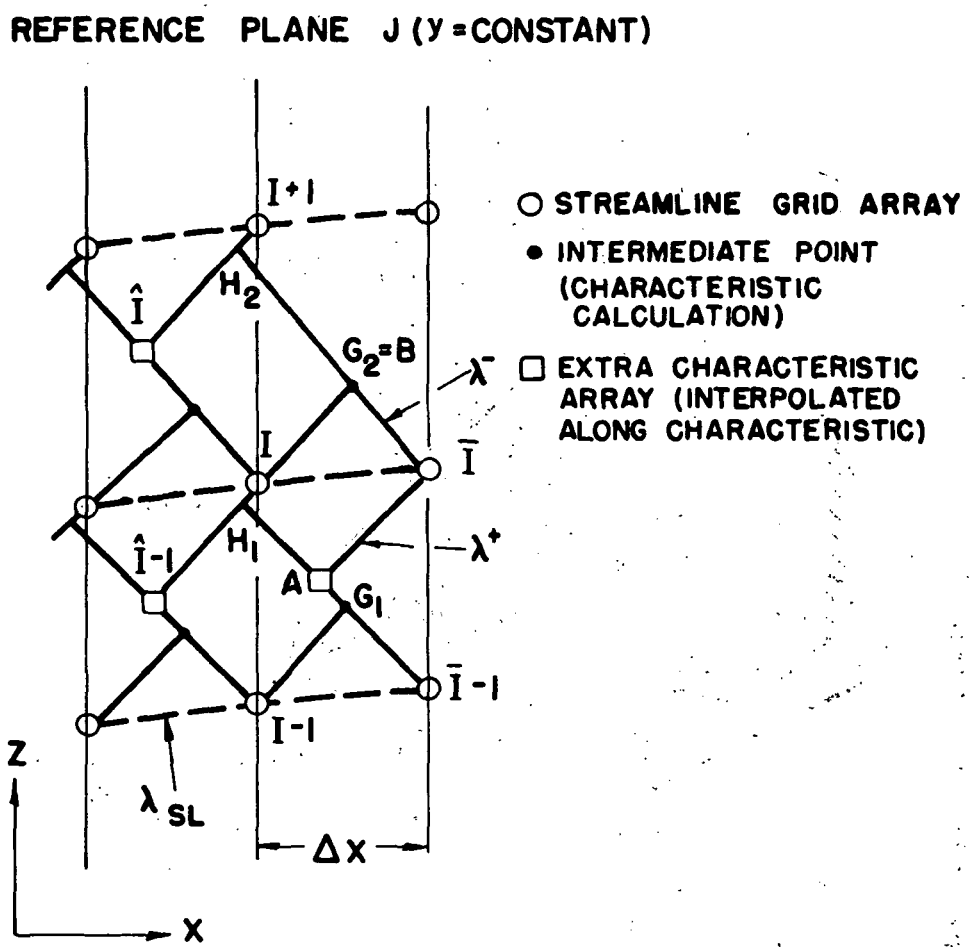

Figure 5.- CHAR3D interior point grid.

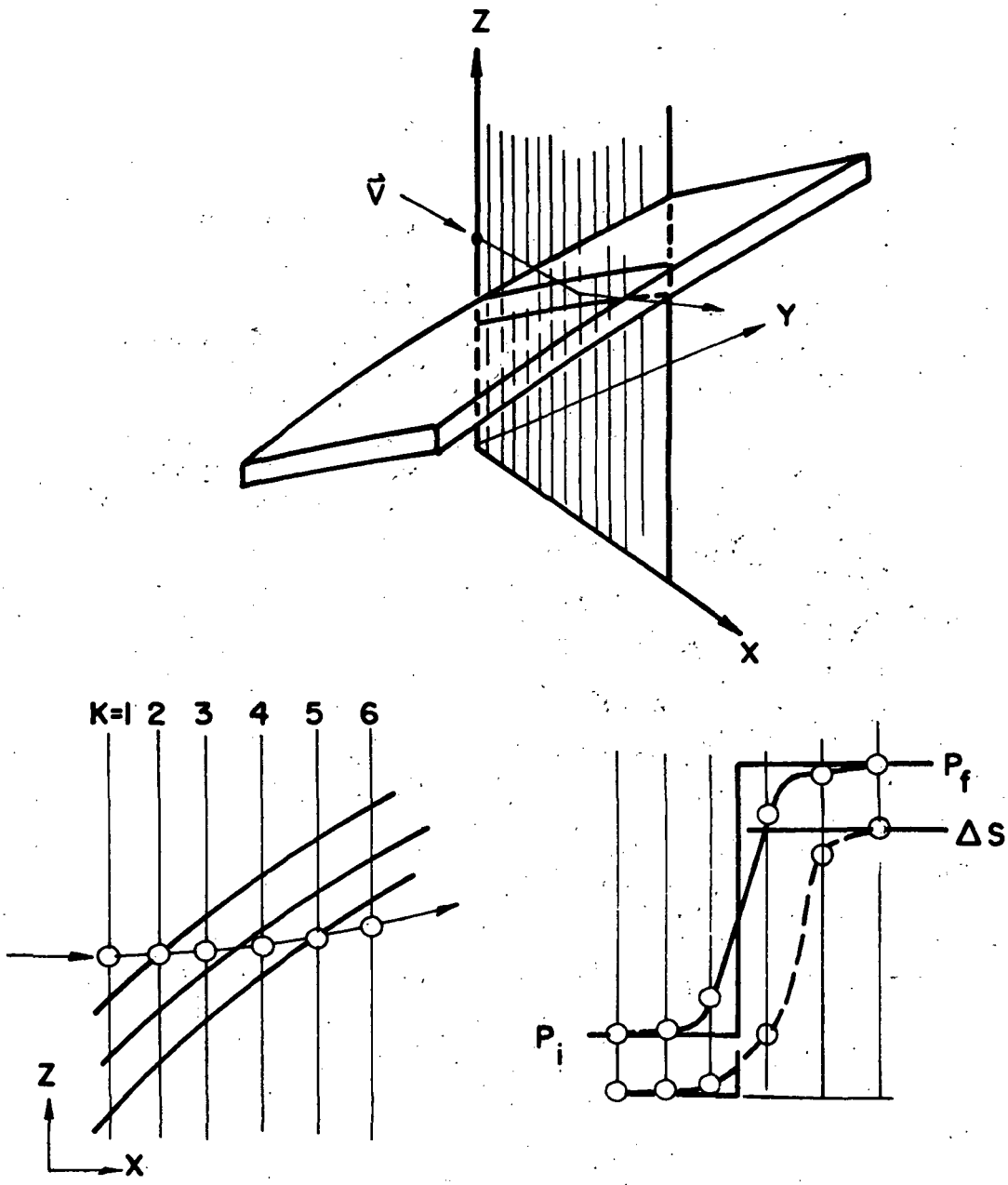

Figure 6.- Entropy calculational procedure. P_i is initial pressure; P_f is final pressure.

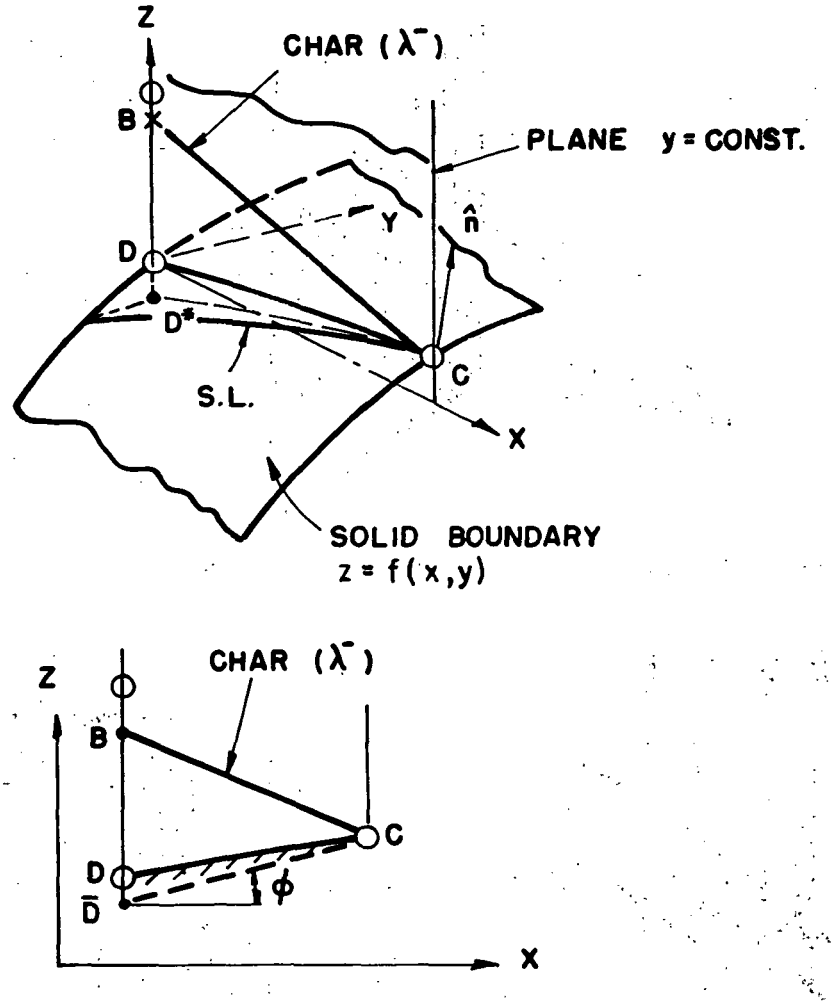

Figure 7.- Solid boundary calculation.

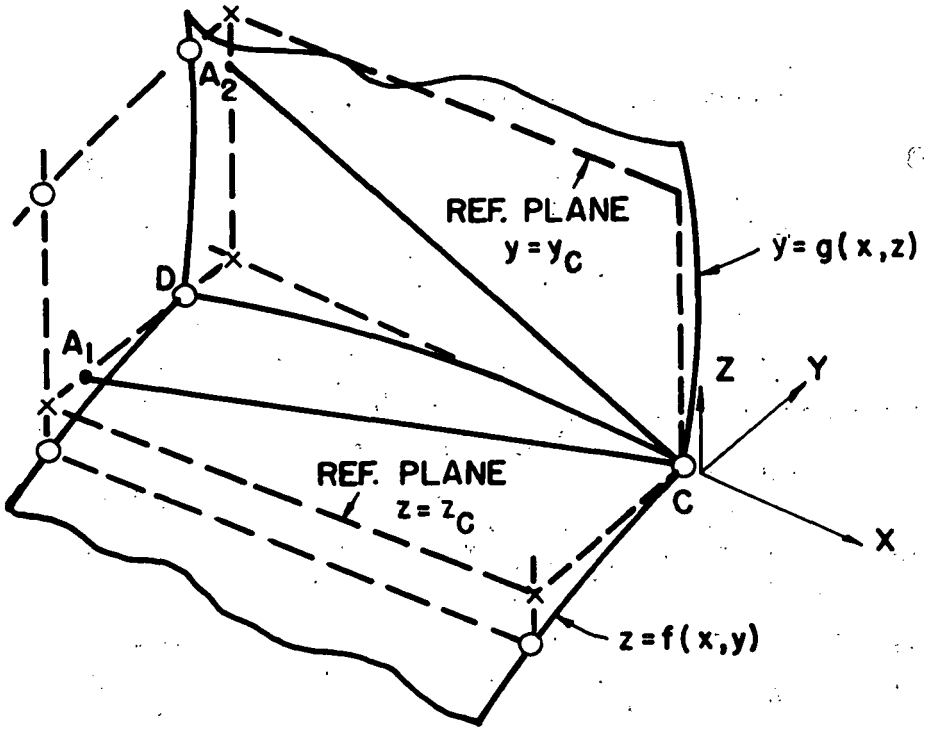

Figure 8.- Internal corner calculation.

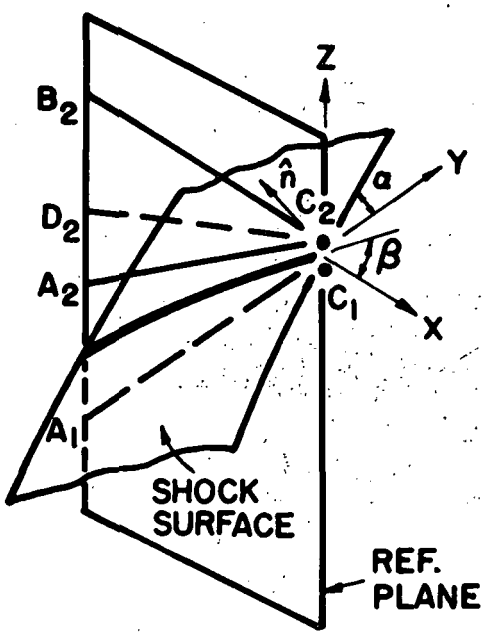

2 IS FREE STREAM SIDE

Figure 9.- Shock surface calculation.

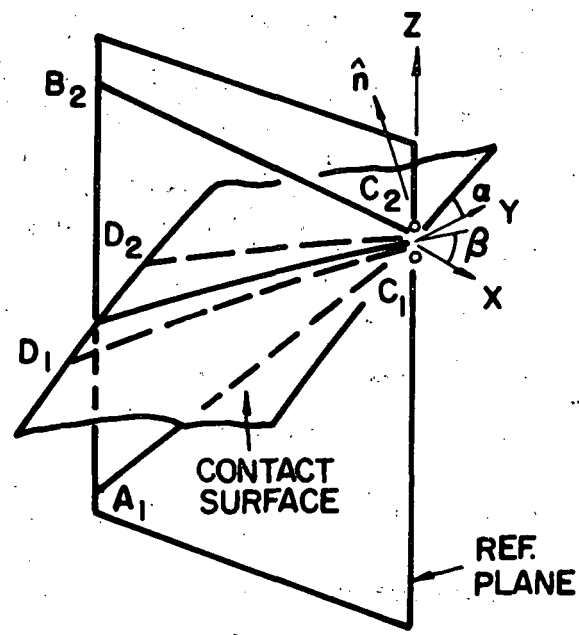

Figure 10.- Contact surface calculation.

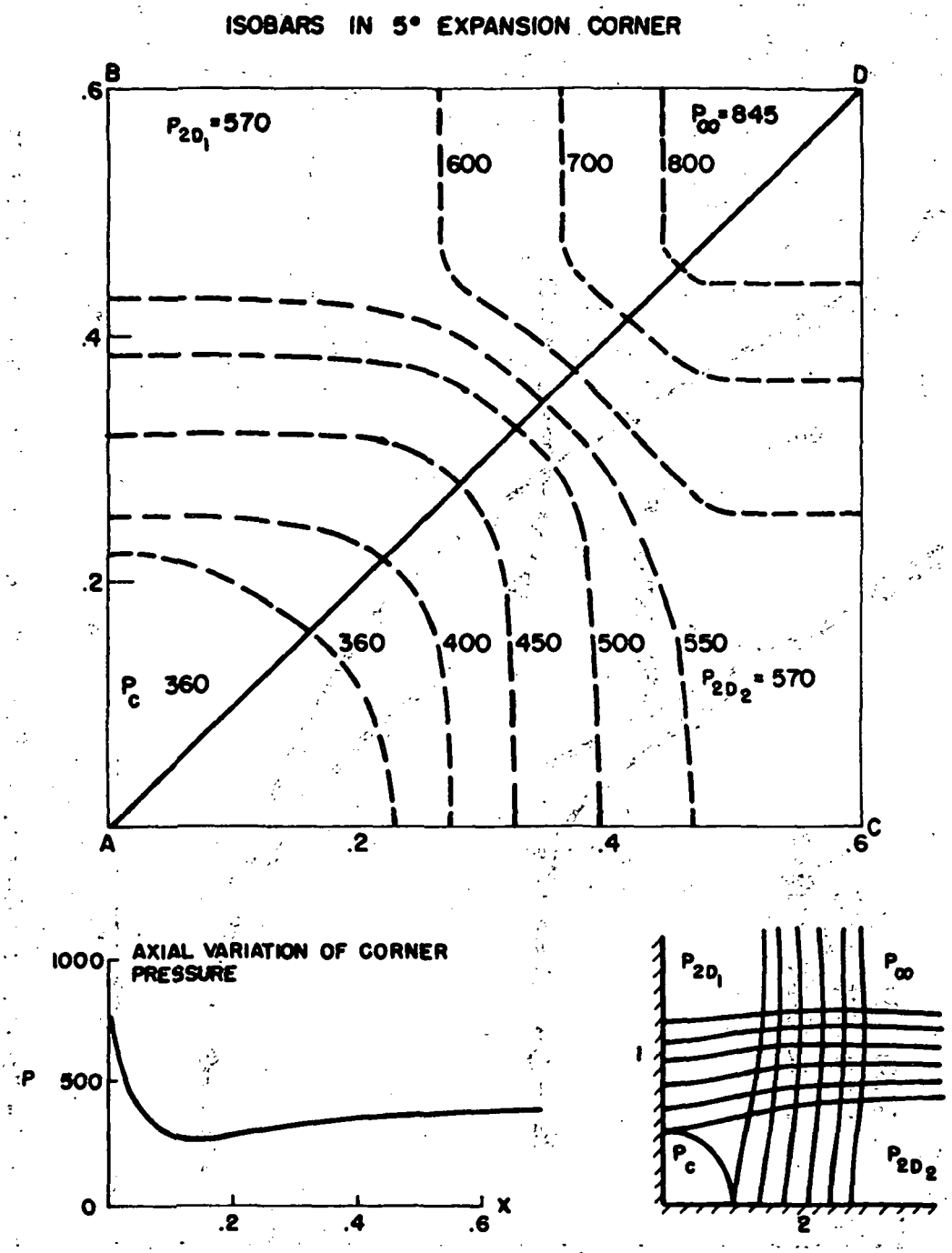

Figure 11.- Results for 5° expansion corner. P_c is corner pressure; P_{2D} is two-dimensional wall pressure.

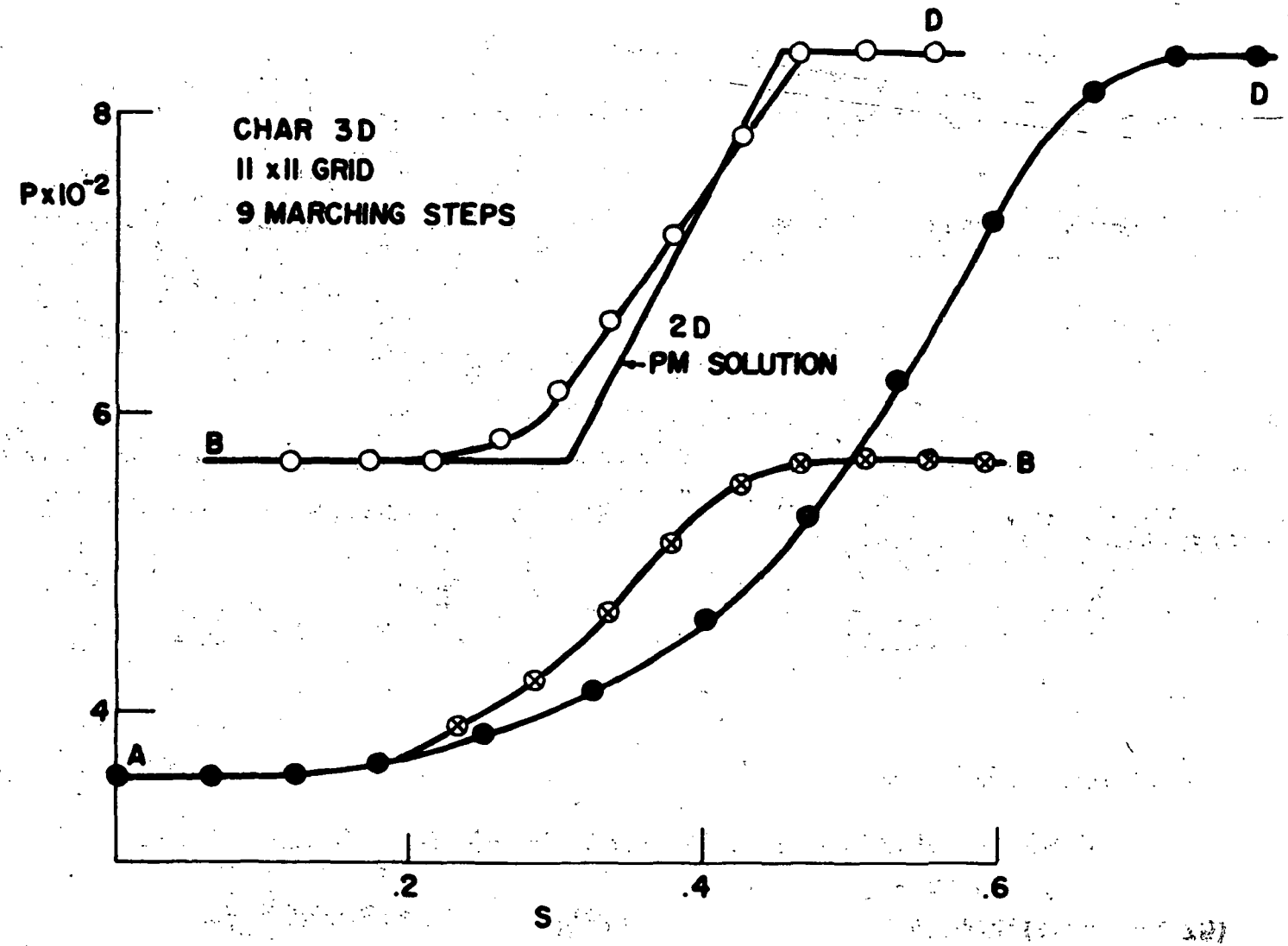

Figure 12.- Pressure distribution for 5^{o} expansion corner. PM means Prandtl-Meyer.

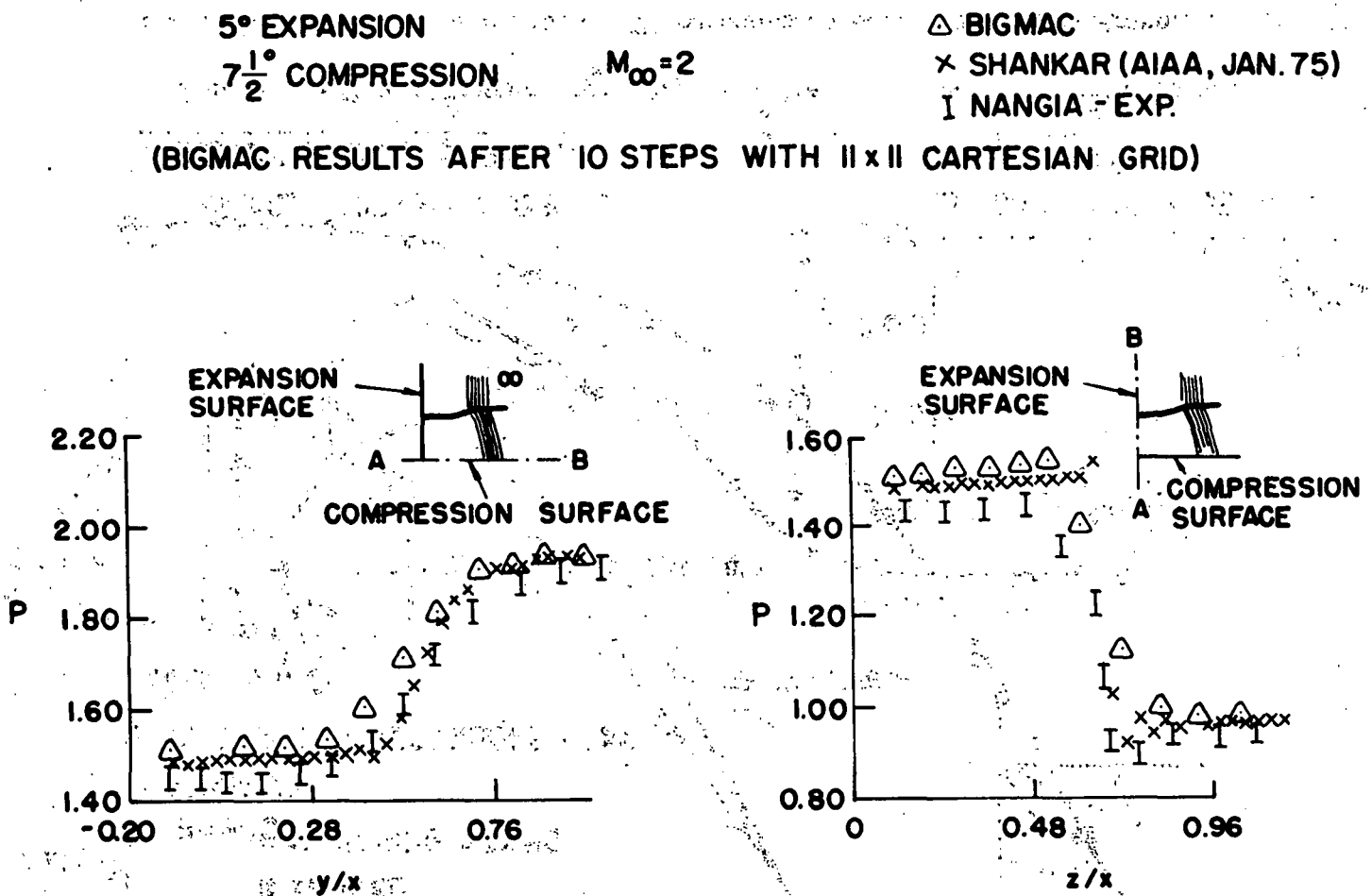

Figure 13.- Results for an expansion-compression corner.

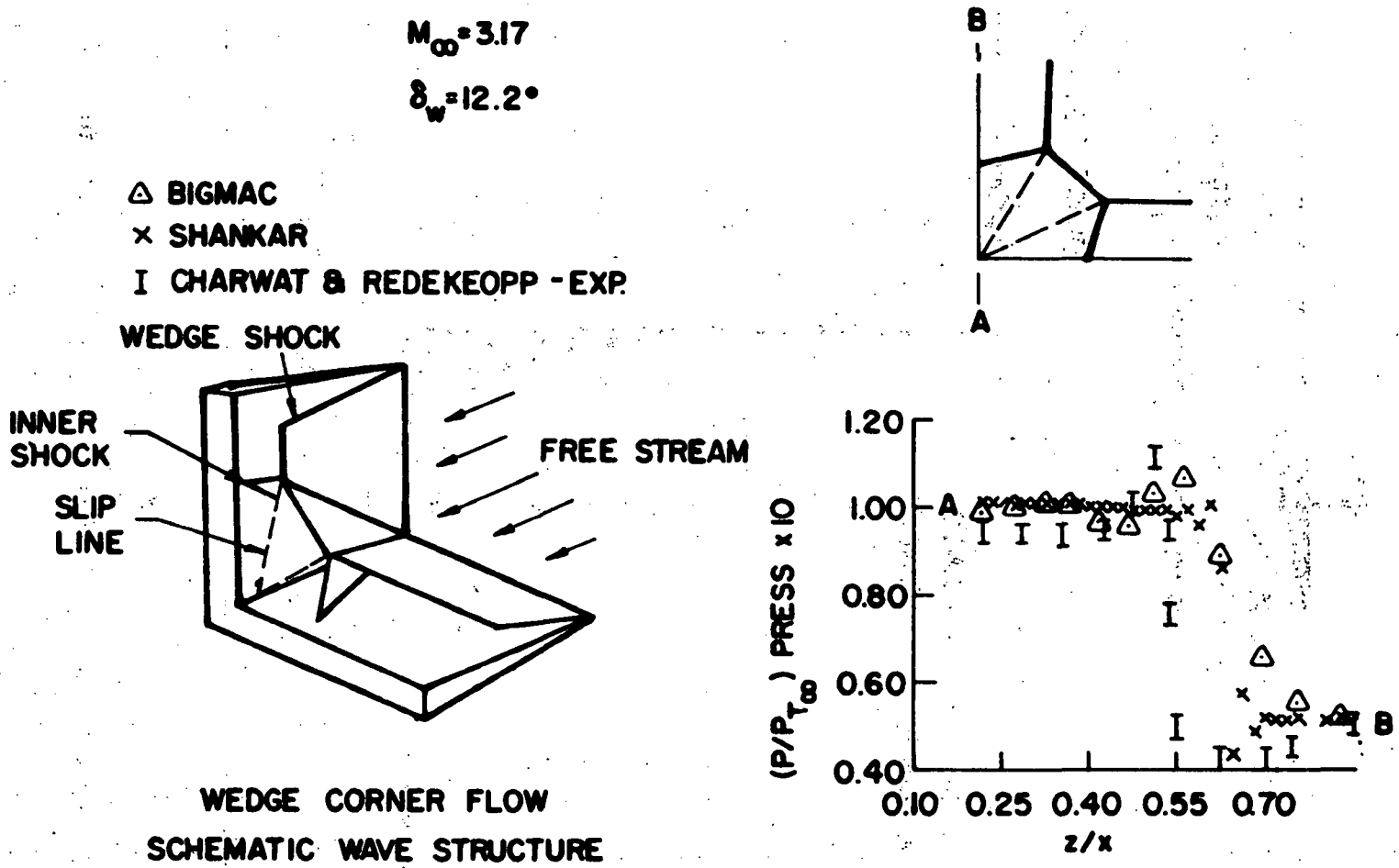

Figure 14.- Compression corner. δ_w is wedge angle; P_{T_∞} is total pressure.

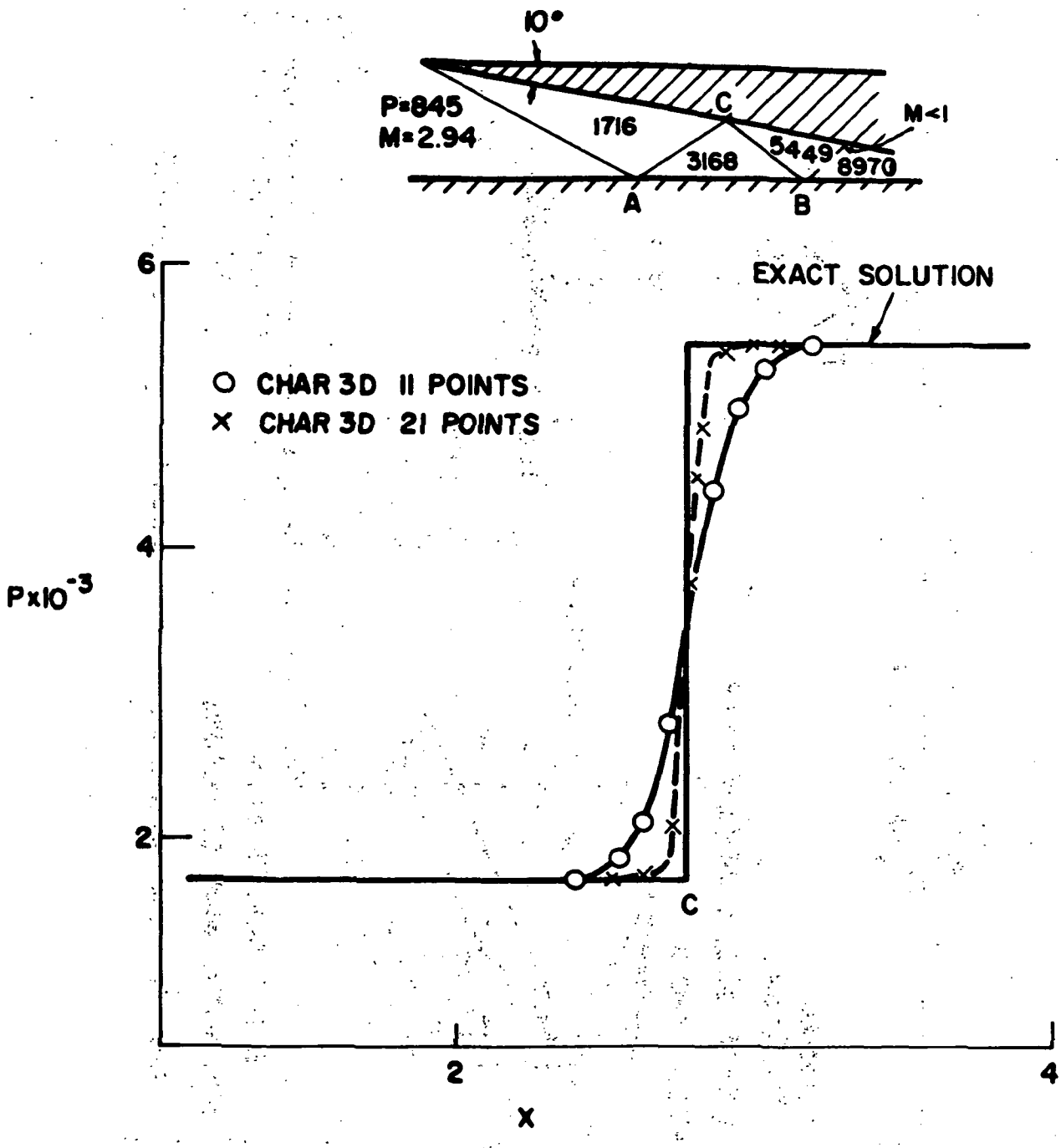

Figure 15.- Upper wall pressure distribution for 10^{o} wedge inlet flow field.

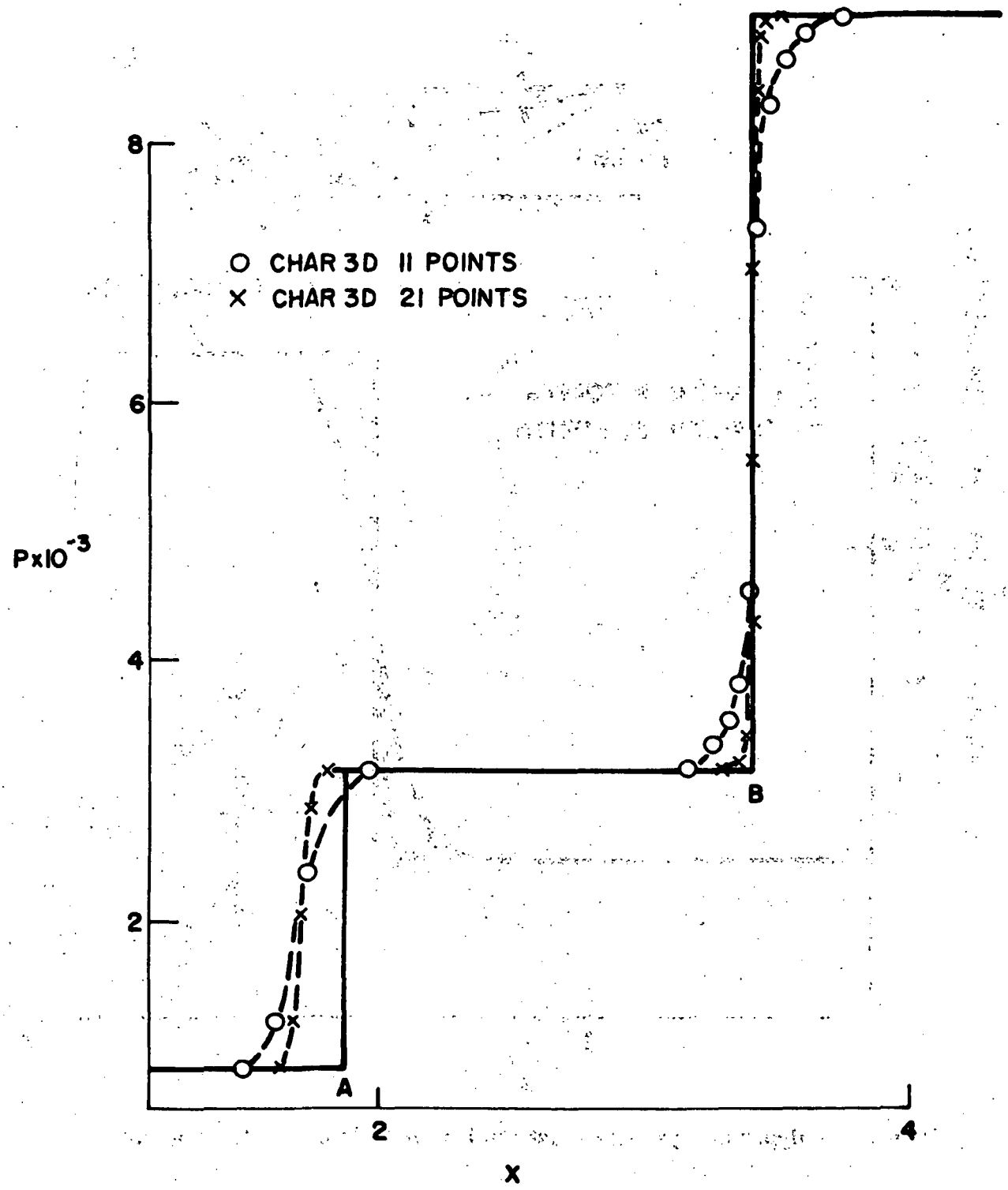

Figure 16.- Lower wall pressure distribution for 10^{o} wedge inlet flow field.

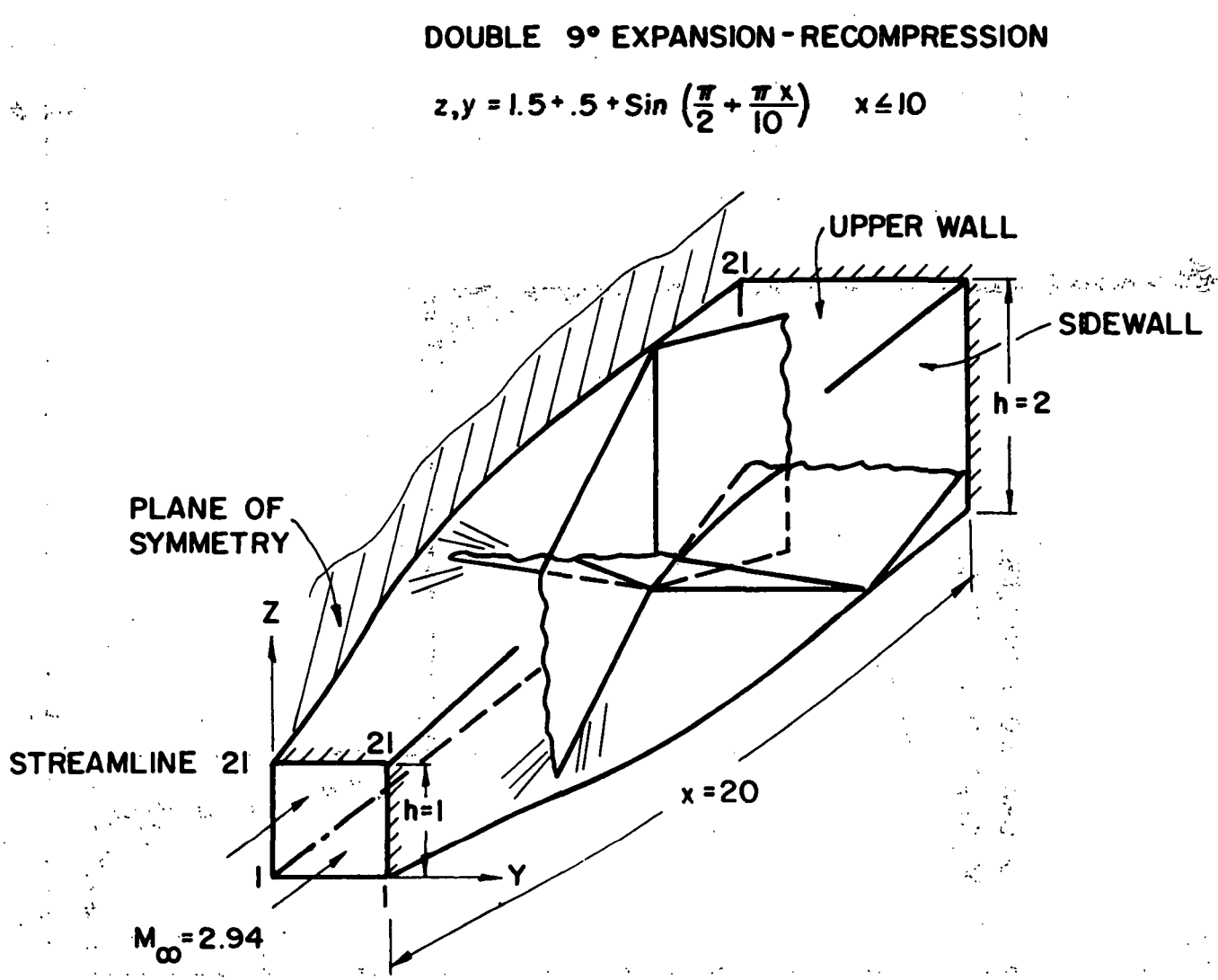

Figure 17.- Square nozzle; h is height.

Figure 18.- Pressure contours on symmetry plane of square nozzle.

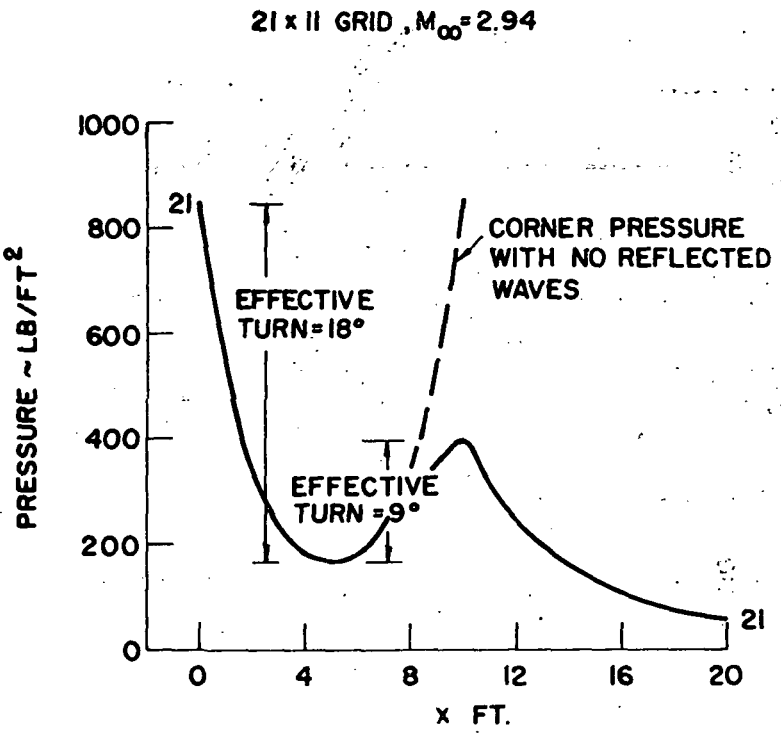

Figure 19.- Streamline pressure distribution at sidewall corner of square nozzle.

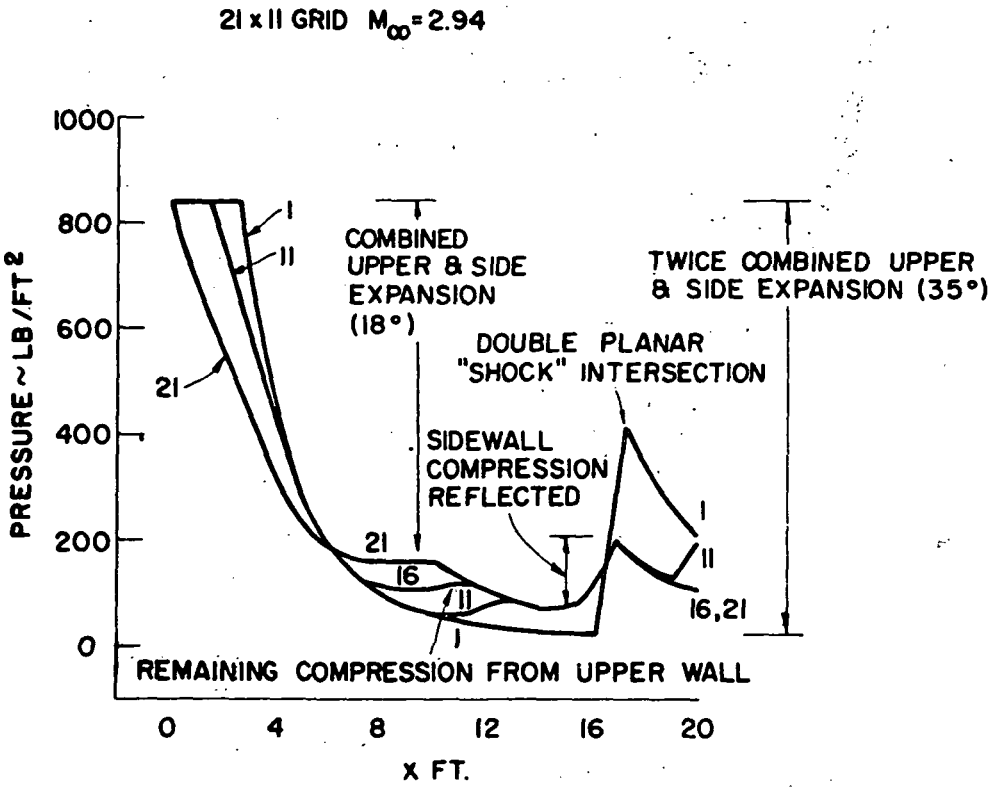

Figure 20.- Streamline pressure distribution in plane of symmetry of square nozzle.

*U.S. GOVERNMENT PRINTING OFFICE: 1975 - 635-275/17